ChemComm

Förster resonance energy transfer involving the triplet state

Journal:	*ChemComm*
Manuscript ID	CC-FEA-02-2023-000748.R1
Article Type:	Feature Article

ARTICLE

Förster resonance energy transfer involving the triplet state

Bahadur Sk[a] and Shuzo Hirata*[a]

Received 00th January 20xx,
Accepted 00th January 20xx

DOI: 10.1039/x0xx00000x

Triplet harvesting is important for high-efficiency optoelectronics devices, time-resolved bioimaging, sensing, and anti-counterfeiting devices. Förster resonance energy transfer (FRET) from the donor (D) to the acceptor (A) is important to efficiently harvest the triplet excitons after a variety of excitations. However, general explanations of the key factors of FRET from the singlet state ($FRET_{S\text{-}S}$) via reverse intersystem crossing and FRET from the triplet state ($FRET_{T\text{-}S}$) have not been reported beyond spectral overlap between emission of the D and absorption of the A. This feature article gives an overview of FRET involving the triplet state. After discussing the contribution of the radiation yield from the state of D considering spin-forbidden factors to FRET, a variety of schemes involving triplet states, such as $FRET_{S\text{-}S}$ via reverse intersystem crossing from the triplet state, dual $FRET_{S\text{-}S}$ and $FRET_{T\text{-}S}$, and selective $FRET_{T\text{-}S}$, are introduced. Representative examples, including the chemical structure and FRET for triplet harvesting, are highlighted using emerging applications in optoelectronics and afterglow imaging. Finally, recent developments of using FRET involving triplet states for high-efficiency optoelectronics devices and time-resolved bioimaging are discussed. This article provides crucial information for controlling state-of-the-art properties using FRET involving the triplet state.

Introduction

Nonradiative energy transfer from the excited state of the donor (D) to the ground state (S_0) of the acceptor (A) is important for enhancing the efficiency of optoelectronic devices,[1-4] solar-energy harvesting,[5,6] photo-induced therapy[7], nonlinear optical devices,[8] bioimaging,[9-12] and anti-counterfeiting devices.[13] Based on conventional photochemistry textbooks,[14] nonradiative energy transfer can be divided into long- and short-range nonradiative energy transfer. Long-range nonradiative energy transfer with a D–A distance (R_{DA}) greater than 10 nm contains a re-absorption process in which the emission from the D is re-absorbed by the A. However, it does not provide important information about nanoscale materials, and it is often called a trivial process.[14] Short-range nonradiative energy transfer induced by R_{DA} of generally less than 10 nm is often of interest because it provides important nanoscale information about the D and A under a variety of conditions of biological media,[9-12] and it is also crucial for enhancing the performance of a variety of optoelectronic devices with thin films.[1-4] Short-range nonradiative energy transfer is generally divided into the following two cases. One of the short-range types of nonradiative energy transfer caused by electronic exchange is called Dexter energy transfer. It occurs between the D and the A when R_{DA} is less than 1 nm because overlapping molecular orbitals between D and A are necessary for electron transfer processes.[15] Dexter energy transfer is an important mechanism because it is related to a variety of effective photo-sensitized reactions for therapy[7] and energy generation[9,10] by photoirradiation. The other type of crucial nonradiative energy transfer is called Förster resonance energy transfer (FRET), which allows energy transfer for a D–A pair with R_{DA} = 1–10 nm.[16-18] The basic theoretical formula was established for FRET in the 1940s.[14,19,20] It inspired many theoretical and experimental scientists to tune the FRET in different mediums, including biological mediums, with a surge in research until the 1990s. The knowledge about FRET has been used for applications, such as ratiometric imaging in biomedia,[9-11] color tuning of flat-panel displays,[1,2] and super-resolution imaging to determine physical information about materials.[21,22]

In addition to generally known FRET, examples of FRET via triplet states and room temperature (RT) FRET from triplet states (i.e., FRET involving triplet states at RT) were reported after the year 2000. The number of recent reports containing FRET involving triplet states at RT has greatly increased because it has application benefits in optoelectronic devices,[3,4] bioimaging,[12] and anti-counterfeiting devices.[13] Contrary to simple FRET without involving triplet states, most reports, including review articles, still have strong aspects regarding introduction of the chemical structures of D–A pairs and a general explanation of the spectral overlap between emission of the D and absorption of the A.[14,19-25] However, it is often difficult to obtain more insights into FRET involving triplet states.

In this feature article, we overview FRET involving triplet states by considering both chemical and theoretical viewpoints. In the second section, we explain FRET from the viewpoint of R_{DA} that allows FRET. In the third section, the kinetic aspects of FRET from the singlet state and triplet state are introduced, particularly from the viewpoint of the D. After briefly introducing important examples of FRET without involving

[a] *Department of Engineering Science and Engineering, The University of Electro-Communications, 1-5-1 Chofugaoka, Chofu, Tokyo 182-8585, Japan. E-mail: shuzohirata@uec.ac.jp*
[b] *† Footnotes relating to the title and/or authors should appear here.*
See DOI: 10.1039/x0xx00000x

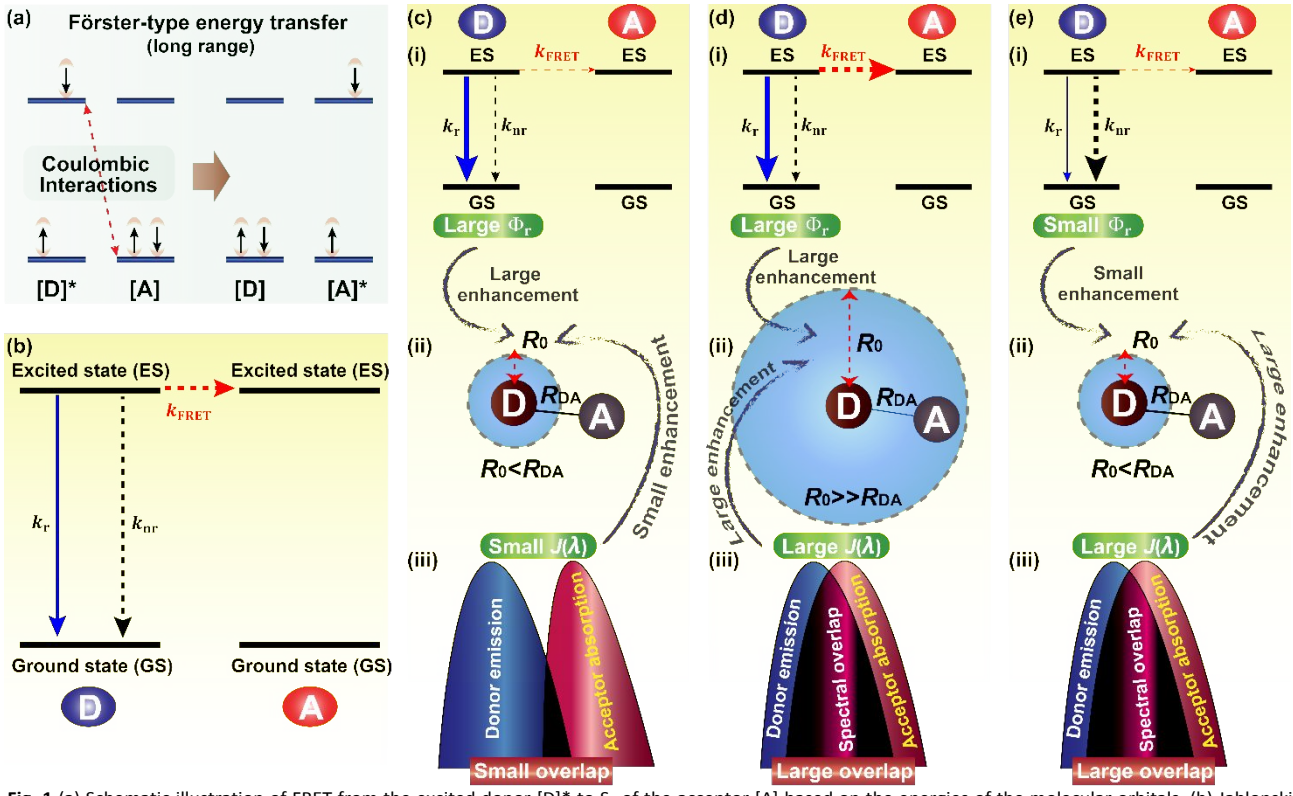

Fig. 1 (a) Schematic illustration of FRET from the excited donor [D]* to S_0 of the acceptor [A] based on the energies of the molecular orbitals. (b) Jablonski diagram showing the relationship among k_r, k_{nr}, and k_{FRET} from the D to the A. (c)–(e) Three cases of FRET from the D to the A: (i) the Jablonski diagram showing k_r, k_{nr}, and k_{FRET} (a thick arrow indicates a large value and a thin arrow indicates a small value), (ii) R_0 and R_{DA}, and (iii) the spectral overlap between the emission of the D and the absorption of the A.

triplet states in the fourth section, we introduce FRET involving triplet states by providing representative chemical examples along with the timeline of their appearance in the fifth to the nineth sections. To carefully guide readers to precise science, representative examples with data showing the direct existence of the corresponding FRET are included in the timeline. The chemicals that have contributed to the recent application progress of FRET involving triplet states are highlighted. Finally, the outlook for FRET involving triplet states is discussed. This feature article provides crucial information for controlling state-of-the-art properties using FRET involving triplet states.

Basic theory of nonradiative energy transfer

FRET occurs because of the interaction between the transition dipole moment of the excited D and that of the ground state A.[14,19,20] Excitation of the D leads to transfer of excitation energy to the A without emission of a photon (Fig. 1a). This energy-transfer process occurs through Coulombic interactions, as given by Förster.[16-18] From the viewpoint of the Jablonski diagram (Fig. 1b), the probability of FRET is expressed using each rate constant from a state, and the FRET efficiency from the state is expressed as

$$\Phi_{FRET} = k_{FRET}/(k_r + k_{nr} + k_{FRET}), \quad (1)$$

where k_r is the radiative rate constant from the state, k_{nr} is the rate of nonradiative transition from the state, and k_{FRET} is the rate of FRET from the state. k_{FRET} is generally expressed as[19]

$$k_{FRET} = (k_r + k_{nr})\left[\frac{R_0}{R_{DA}}\right]^6, \quad (2)$$

where R_0 is the Förster radius, which indicates the distance between the D and the A with energy-transfer efficiency of 50%. R_0 is generally given by[19]

$$R_0 = \left(\frac{9000(\ln 10)}{128\pi^5 N_A n^4}\kappa^2 \Phi_r J(\lambda)\right)^{1/6}, \quad (3)$$

where Φ_r is the radiation quantum yield of the D in the absence of an A, n is the refractive index of the medium, N_A is Avogadro's number, κ^2 is the dipolar orientation factor between the D and the A, and $J(\lambda)$ is the spectral overlap integral between the emission spectrum of the D and the absorption spectrum of the A. $J(\lambda)$ can be expressed as[19]

$$J(\lambda) = \frac{\int_0^\infty F_D(\lambda)\varepsilon_A(\lambda)\lambda^4 d\lambda}{\int_0^\infty F_D(\lambda) d\lambda}, \quad (4)$$

where $F_D(\lambda)$ is the normalized emission intensity of the D in the absence of the A and ε_A is the absorption coefficient of the A at wavelength λ (in nm). From equations (2) and (3), k_{FRET} is expressed as

$$k_{FRET} = k_r J(\lambda)\frac{9000(\ln 10)\kappa^2}{128\pi^5 N_A n^4}\left[\frac{1}{R_{DA}}\right]^6. \quad (5)$$

Equation (5) indicates that k_{FRET} is proportional to k_r when R_{DA} is the same, for the conditions using similar κ^2 and n. The simplified expression for R_0 (in nm) is

$$R_0 = 0.0211 \times \sqrt[6]{\kappa^2 n^{-4} \Phi_r J(\lambda)}. \quad (6)$$

From equations (1)–(4), Φ_{FRET} can be expressed as

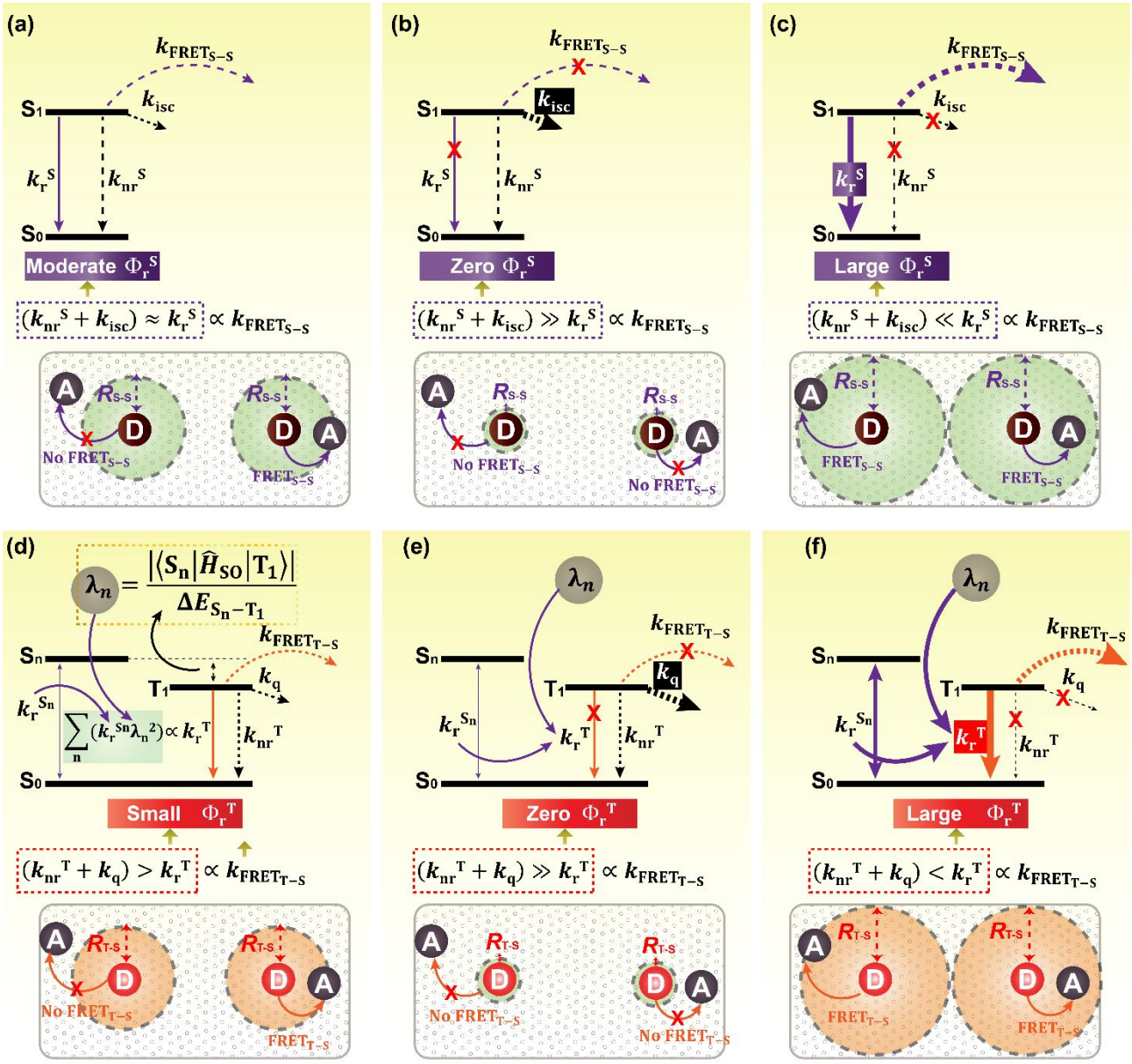

Fig. 2 Schematic illustrations show the relationship between the kinetics from excited state of D and the magnitude of FRET efficiency. (a) The case in which the moderate Φ_r^S of the D allows $FRET_{S-S}$. (b) The case in which the zero Φ_r^S of the D does not allow $FRET_{S-S}$ because of the large $(k_{nr}^S + k_{isc})$ compared with (a). (c) The case in which the large Φ_r^S of the D greatly contributes to the enhancement of $FRET_{S-S}$ efficiency because of the enhancement of k_r^S compared with (a). (d) The case in which the small Φ_r^T of the D allows a small possibility for $FRET_{T-S}$ because of the minimized k_q compared with (e). (e) The case in which the zero Φ_r^T of the D does not allow $FRET_{T-S}$ because of the significantly large k_q. (f) The case in which the large Φ_r^T of the D with facilitated k_{nr}^T compared with (d) greatly contributes to the enhancement of $FRET_{T-S}$ efficiency.

$$\Phi_{FRET} = \frac{R_0^6}{R_0^6 + R_{DA}^6}. \quad (7)$$

From equation (7), if R_0 is smaller than the R_{DA}, the FRET efficiency significantly decreases (Fig. 1c(ii) and 1e(ii)). If R_0 is larger than R_{DA}, the FRET efficiency greatly increases (Fig. 1d(ii)). Therefore, it is important to control R_0 and R_{DA} to enhance the efficiency of FRET.

To enhance R_0 for large Φ_{FRET}, increasing $(\Phi_r)^{1/6}$ and $J(\lambda)^{1/6}$ is crucial based on equation (3). When two cases with comparable Φ_r values (Fig. 1c(i) and 1d(i)) are considered, a small $\varepsilon_A(\lambda)$ and small overlap between the emission and absorption spectra result in a small $J(\lambda)$ (Fig. 1c(iii)). However, a large $\varepsilon_A(\lambda)$ and large overlap between the emission and absorption spectra result in a large $J(\lambda)$ (Fig. 1d(iii)). Because the small $J(\lambda)$ induces smaller R_0, a D-A pair with a large $J(\lambda)$ (Fig. 1d(ii)) increases the possibility of FRET compared with the D-A pair with a small $J(\lambda)$ (Fig. 1c(ii)). Although the increase of $J(\lambda)$ is often considered from the viewpoints of $\varepsilon_A(\lambda)$ and the overlap between the emission and absorption spectra, Φ_r is also crucial to consider. For instance, when two cases with comparable $J(\lambda)$ values are considered (Fig. 1d(iii) and 1e(iii)), D with much smaller Φ_r (Fig. 1e(i)) does not contribute to enhancement of R_0 based on equation (3). This greatly decreases the probability of FRET because of the increase of the probability of $R_0 < R_{DA}$ (Fig. 1e(ii)). From equations (3) and (6), κ^2 also contributes to R_0, and it depends on the orientation between the D and the A. However, κ^2 can greatly change under limited specialized conditions, such as for co-crystals composed of the D and A and a single molecule in which the D and A are chemically connected using a rigid non-conjugated structure.

For general materials including the isotropic condition, $J(\lambda)$ and Φ_r are generally crucially independent of the orientation between the D and the A for considering FRET.

FRET from the singlet state and triplet state

Although $J(\lambda)$ and Φ_r are two representative factors to control R_0, $J(\lambda)$ has been well explained in previous textbooks[14,19,20] and the literature.[23,24] However, the contribution of the Φ_r of D to FRET from singlet and triplet states has not been developed and discussed in textbooks or review articles. Therefore, we focus on the contribution of the Φ_r to FRET in this paper, when the D-A pair has the same $J(\lambda)$. FRET between the lowest singlet excited state (S_1) of the D ($^1D^*$) and S_0 of the A (^1A) is generally expressed as

$$^1D^* + {}^1A \rightarrow {}^1D + {}^1A^* \quad (8)$$

where ^1D and $^1A^*$ are S_0 of the D and S_1 of the A, respectively. If FRET between the lowest triplet state (T_1) of the D ($^3D^*$) and ^1A is generally possible, it can be expressed as

$$^3D^* + {}^1A \rightarrow {}^1D + {}^1A^* \quad (9)$$

Equation (8) indicates common FRET, which we define as $FRET_{S\text{-}S}$ in this paper. When $FRET_{S\text{-}S}$ is considered, Φ_r in equations (3) and (6) corresponds to the fluorescence yield (Φ_r^S), and a large Φ_r^S increases R_0 of $FRET_{S\text{-}S}$ ($R_{S\text{-}S}$) for efficient $FRET_{S\text{-}S}$ based on equation (6). Φ_r^S from S_1 is generally expressed using the radiative rate constant from S_1 (k_r^S), the nonradiative rate constant from S_1 to S_0 (k_{nr}^S), and the rate of intersystem crossing from S_1 to the triplet states (k_{isc}): $\Phi_r^S = k_r^S/(k_r^S + k_{nr}^S + k_{isc})$ (Fig. 2a).[14,26] For instance, consider that materials D and A are dispersed in an amorphous host. One A is located inside the Förster radius for $FRET_{S\text{-}S}$ ($R_{S\text{-}S}$) of a D while another A is not inside the $R_{S\text{-}S}$ of another D (Fig. 2a). In this situation, the $FRET_{S\text{-}S}$ efficiency is not high on average. When two Ds with similar k_r^S are compared (Fig. 2a and 2b), the D with much larger ($k_{nr}^S + k_{isc}$) results in less $FRET_{S\text{-}S}$ (Fig. 2b). Although $k_{FRET_{S-S}}$ is proportional to k_r^S based on equation (5), $k_{FRET_{S-S}}$ is often difficult to increase up to the magnitude of ($k_{nr}^S + k_{isc}$) because the k_r^S required to facilitate $k_{FRET_{S-S}}$ is much smaller compared with the large ($k_{nr}^S + k_{isc}$). Thus, the large ($k_{nr}^S + k_{isc}$) is still much larger than $k_{FRET_{S-S}}$, and because ($k_{nr}^S + k_{isc}$) $\gg$ k_r^S, the much smaller Φ_r^S results in much smaller $R_{S\text{-}S}$. This significantly decreases the average $FRET_{S\text{-}S}$ efficiency because most of A is outside of the $R_{S\text{-}S}$ of D (Fig. 2b). A variety of simple aromatic fused rings with a symmetrically forbidden S_1-S_0 transition have small k_r^S, resulting in $k_{isc} > k_r^S$ and inducing small Φ_r^S.[28] Therefore, simple aromatic fused rings are not suitable for $FRET_{S\text{-}S}$. For chromophores containing heavy atoms, k_{isc} increases because of the heavy atom effect and Φ_r^S becomes small because $k_{isc} > k_r^S$. For heavy-atom-free chromophores with large spin-orbit coupling based on the El-Sayed rule, Φ_r^S becomes zero or small because $k_{isc} > k_r^S$. Therefore, these chromophores are not suitable for efficient $FRET_{S\text{-}S}$. When two Ds with similar ($k_{nr}^S + k_{isc}$) are compared (Fig. 2a and 2c), the D with larger k_r^S allows for more $FRET_{S\text{-}S}$. Because $k_{FRET_{S-S}}$is proportional to k_r^S and k_r^S is much larger than ($k_{nr}^S + k_{isc}$), $k_{FRET_{S-S}}$ can easily be increased to magnitudes much greater than ($k_{nr}^S + k_{isc}$), owing to the large magnitude of k_r^S. Therefore, when $k_r^S \gg (k_{nr}^S + k_{isc})$, the larger Φ_r^S results in larger $R_{S\text{-}S}$. This significantly increases the average $FRET_{S\text{-}S}$ efficiency because most of A is inside of the $R_{S\text{-}S}$ of D (Fig. 2c). Because a D showing blue and green fluorescence often has small k_{nr}^S based on the energy gap law,[27] it often exhibits a large Φ_r^S when heavy atoms are not contained in the D, greatly facilitating k_{isc}. Therefore, various chromophores with blue and green fluorescence may enable efficient $FRET_{S\text{-}S}$.

For FRET from T_1, we define the reaction of equation (9) as $FRET_{T\text{-}S}$ in this paper. For $FRET_{T\text{-}S}$, Φ_r in equations (3) and (6) corresponds to the radiation yield from T_1 (Φ_r^T) (Fig. 2c). Large Φ_r^T increases R_0 of $FRET_{T\text{-}S}$ ($R_{T\text{-}S}$) for efficient $FRET_{T\text{-}S}$ based on equation (6). It should be noted that Φ_r^T is different from the phosphorescence yield (Φ_P): $\Phi_r^T = \Phi_P/\Phi_{ISC}$, where Φ_{ISC} is the yield of triplet generation from singlet states. Using the radiative rate constant from T_1 of the D (k_r^T), the nonradiative transition rate from T_1 of the D (k_{nr}^T), and the quenching rate from T_1 of the D caused by the interaction between the D and the host matrix (k_q), Φ_r^T is expressed as $\Phi_r^T = k_r^T/(k_r^T + k_{nr}^T + k_q)$ (Fig. 2c).[28] $FRET_{T\text{-}S}$ might be an impossible process when the general spin preservation rule is considered by just observing the shape of equation (9). However, $FRET_{T\text{-}S}$ is logically allowed for the following reasons. k_r^T has a certain value by mainly borrowing a contribution of the radiative rate from a variety of singlet states (S_n) to S_0 (k_r^{Sn}) (Fig. 2d) with a percentage of λ_n^2,[28] where λ_n is approximately expressed as $\lambda_n \simeq \langle T_n | \hat{H}_{SO} | S_0 \rangle / \Delta E_{S_n - T_1}$ using the spin-orbit coupling between S_n and T_1 ($\langle T_n | \hat{H}_{SO} | S_0 \rangle$) and the energy difference between S_n and T_1 ($\Delta E_{S_n - T_1}$) (Fig. 2d).[28-32] In other words, k_r^T is enhanced by approximate multiplication of k_r^{Sn} and λ_n^2 (Fig. 2d). Therefore, k_r^T has slight singlet–singlet transition nature with the possibility of λ_n^2, slightly breaking the forbidden nature of the reaction regarding equation (9). When two Ds with similar k_r^T are compared (Fig. 2d and 2e), the D with larger ($k_{nr}^T + k_q$) results in a lower $FRET_{T\text{-}S}$ efficiency (Fig. 2e). Notably, solids containing a heavy-atom-free D often show zero Φ_r^T at RT because a significant increase in k_q is often observed at RT (Fig. 2e).[28,33,34] In this situation, $k_{FRET_{T-S}}$ is still much less than the large k_q because $k_{FRET_{T-S}}$ is proportional to the small k_r^T ($\ll k_q$) based on equation (5). Therefore, $FRET_{T\text{-}S}$ does not occur at RT because of the large k_q at RT, even when the D-A pair has a large $J(\lambda)$ between the phosphorescence of D and absorption of A. However, when the D is dispersed in an appropriate host to allow for strong triplet confinement, k_q significantly decreases and exhibits a similar or lower magnitude compared with k_r^T and k_{nr}^T of heavy-atom-free chromophores (Fig. 2d).[33] The significant suppression of k_q breaks the zero Φ_r^T and slightly increases $R_{T\text{-}S}$ to open a window of $FRET_{T\text{-}S}$. However, k_{nr}^T is often larger than k_r^T for heavy-atom-free chromophores. When k_r^T increases without an increase in k_{nr}^T, Φ_r^T also increases, which enhances $R_{T\text{-}S}$ for more efficient $FRET_{T\text{-}S}$ (Fig. 2f). Because the selective enhancement of k_r^T without increasing k_{nr}^T has been reported by increasing k_r^{Sn} and λ_n,[28] more chemical designs that enable more $R_{T\text{-}S}$ at RT are anticipated.

In the following sections, after briefly explaining conventional FRET and FRET at liquid-nitrogen temperature, we introduce the occurrence of FRET involving the triplet state at RT, such as $FRET_{S\text{-}S}$ via reverse intersystem crossing (RISC) from the triplet state, dual $FRET_{S\text{-}S}$ and $FRET_{T\text{-}S}$, and selective $FRET_{T\text{-}S}$, which have attracted much attention since 2000.

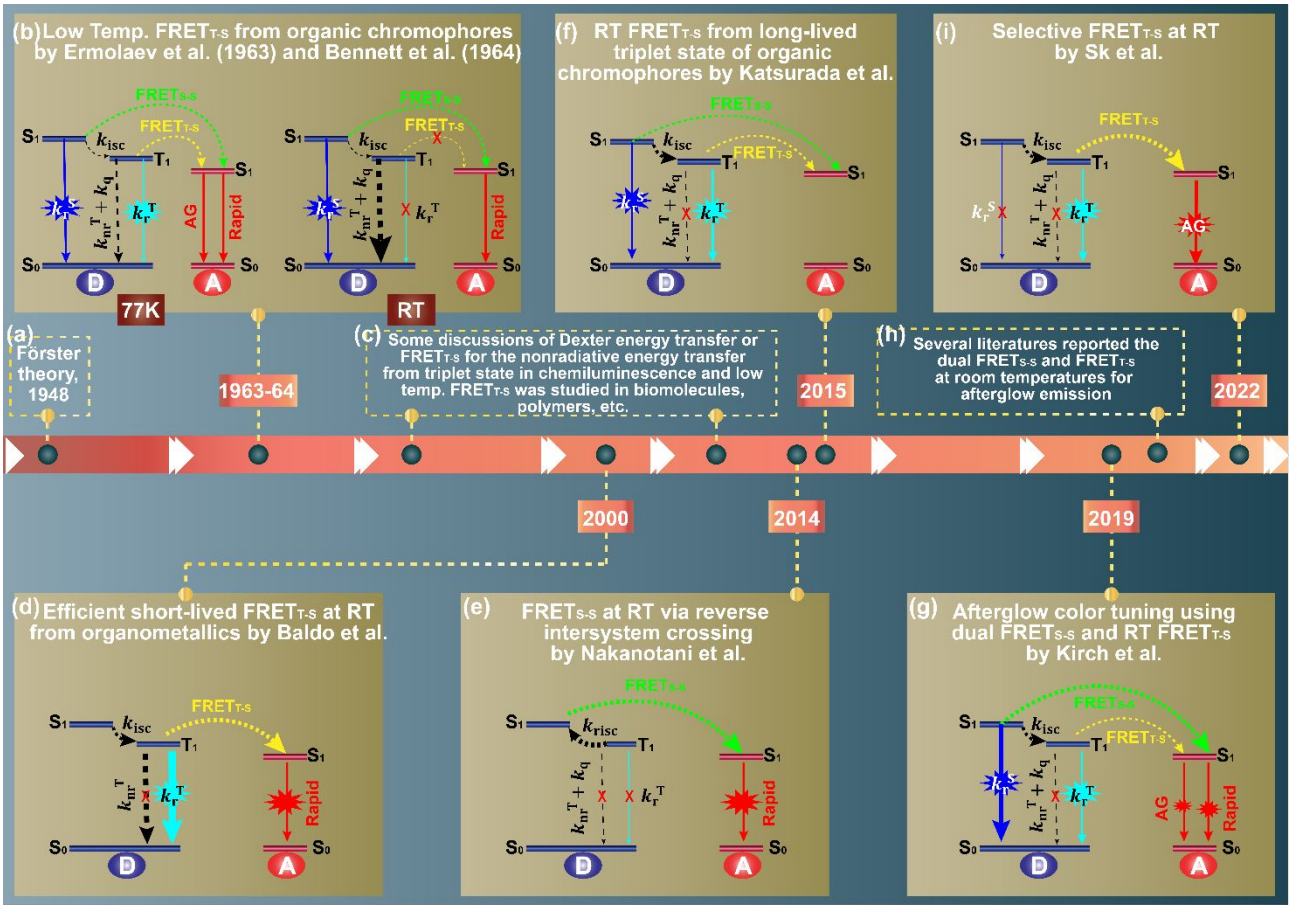

Fig. 3 Schematic illustration of the timeline of FRET involving triplet states. The representative reports in this figure were determined by the presence of the following evidence for very FRET and exclude other possibilities. The evidence for FRET$_{T-S}$ includes the phosphorescence decay change of the D in the presence and absence of the A and/or precise R_{T-S} data determined by Φ_r^S and $J(\lambda)$ without assumption to verify no possibility of electron-transfer-quenching processes to exclude a possibility of Dexter energy transfer process.

FRET$_{S-S}$

Since the development of Förster theory (a in Fig. 3), many researchers have used FRET$_{S-S}$ as a spectroscopic ruler[35] in biological systems to determine the distance between the two terminals linked with the D and A in a medium, as well as in chemical and biological imaging[36] and optoelectronic devices. Over the past few decades, researchers have focused on biological applications, especially imaging and sensing via FRET$_{S-S}$.[9-11] Efficient FRET$_{S-S}$ has also been used for color tuning of electroluminescence devices with a thin emitting film, even when the thickness of the film was less than 100 nm.[1,2] Since 2000, reversible photo-induced FRET$_{S-S}$ from fluorescence molecules as a D and photochromic diarylethenes as an A in single molecules has been reported.[21,37] This kind of reversible fluorescence switching allows photo-activated localization microscopy which is known as one of technique to allow super-resolution imaging.[22]

Low-temperature FRET$_{T-S}$

Although FRET$_{S-S}$ has been used for a variety of applications for several dozens of years, FRET$_{T-S}$ from of heavy atom-free materials has often been considered to be a spin-forbidden process at RT. Because nonradiative triplet decay is also thermally activated in many cases, phosphorescence is observed at 77K because of a large suppression of k_q. Only a few examples of heavy atom-free materials with RT phosphorescence (RTP) have been reported under specialized conditions using crystals and caged structures in 1900s.[38,39] The distinct appearance of triplet radiation at 77 K, which is probably because of large suppression of k_q at 77 K, allows FRET$_{T-S}$ at 77 K (b in Fig. 3).[40] FRET$_{T-S}$ of several chromophores, such as triphenylamine, tryptophan, *p*-phenylbenzaldehyde, *N*,*N*-dimethylaniline, and fluorescein, to several acceptor units at 77 K (or 90 K) was first experimentally observed by Ermolaev and Sveshnikova.[40] A good correlation between the experimentally determined R_0 with that predicted from Förster's expressions indicates FRET$_{T-S}$.

Bennett et al. reported FRET$_{T-S}$ from the phenanthrene-d_{10} as a D to the rhodamine B as an A at 77 K (Figs. 3b and 4a).[41] The significant spectral overlap and triplet radiation because of suppression of the nonradiative processes of deuterated phenanthrene at 77 K suggested the possibility of FRET$_{T-S}$ (Fig. 4b).[41] The decrease of the phosphorescence lifetime with increasing concentration of the A also suggested the existence of FRET$_{T-S}$ (Fig. 4c). They carefully estimated Φ_{ISC} by measuring the dependence of the ratio of the fluorescence intensity to the phosphorescence intensity on the concentration of the A to

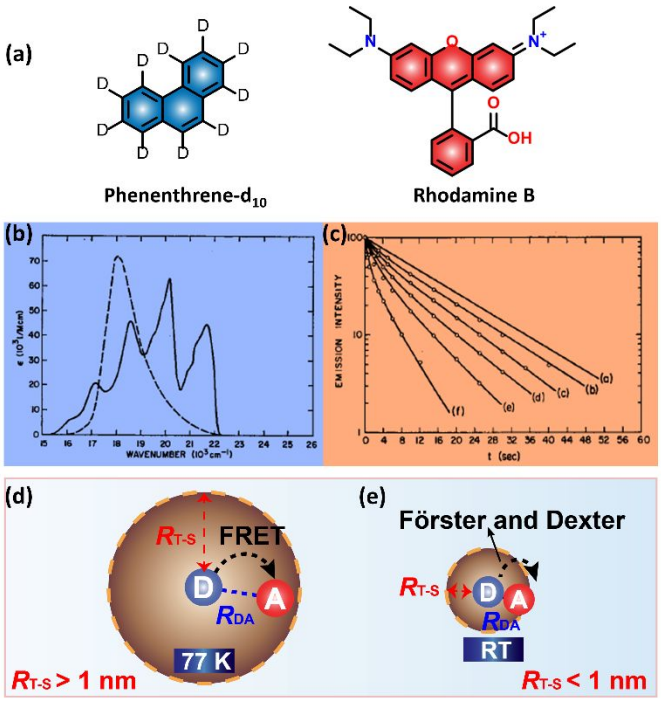

Fig. 4 (a) Molecular structures of phenanthrene-d_{10} as a D and rhodamine B as an A. (b) Spectral overlap of the phosphorescence spectrum of the D at 77 K and the absorption spectrum of the A. (c) Phosphorescence decay profiles of the D at 77 K with increasing concentration of the A (from a to f). The large spectral overlap and the decrease in the phosphorescence lifetime in the presence of the A at 77 K indicates $FRET_{T\text{-}S}$ from the D to the A at 77 K. Reproduced with permission from Elsevier Publishing.[41] Greatly different $R_{T\text{-}S}$ values between (d) 77 K and (e) RT under ambient conditions when the same heavy-atom-free organic chromophores were used as the D and A.

confirm $\Phi_r^T = k_r^T/(k_r^T + k_{nr}^T + k_q)$. Because of determination of Φ_r^T, R_0 = 4.6 nm for $FRET_{T\text{-}S}$ ($R_{T\text{-}S}$) at 77K was determined to finally confirm $FRET_{T\text{-}S}$ at 77K. Furthermore, the phosphorescence lifetime of the D, triphenylene-d_{12}, in the presence of the energy acceptor A, rhodamine B, confirmed $FRET_{T\text{-}S}$ at 77 K.[42]

Chromophores based on biomolecules, such as DNA, proteins (amino acids), enzymes, and chlorophyll, show emission from both the singlet and triplet states at low temperature. Owing to the large amount of radiation (Φ_r^T) from the triplet state at 77 K, $FRET_{T\text{-}S}$ in biomolecules has been studied at liquid-nitrogen temperature. For example, delayed fluorescence has been obtained from DNA–acridine dye complexes owing to the long-range interaction between two transition dipole moments at 77 K, which is $FRET_{T\text{-}S}$.[43,44] Low-temperature $FRET_{T\text{-}S}$ in the vitamin B6 group from the pyridoxal triplet state to the singlet state of L-kynurenine, a metabolite of the amino acid L-tryptophan, has been reported at 77 K.[45] The significant overlap between the phosphorescence spectrum of pyridoxal and the absorption spectrum of L-kynurenine, along with the decrease of the phosphorescence lifetime of pyridoxal with increasing concentration of L-kynurenine, indicated $FRET_{T\text{-}S}$. Furthermore, low-temperature $FRET_{T\text{-}S}$ in a protein at 77 K has been investigated, in which the tryptophan residue of chymotrypsin was the triplet energy D and proflavin was the A in the active site of the protein.[46] Delayed fluorescence from proflavin was obtained owing to $FRET_{T\text{-}S}$, with a yield of 80% calculated by the ratio between the tryptophan phosphorescence and the fluorescence in the presence of the binding acceptor chromophore proflavin. Competitive $FRET_{S\text{-}S}$ pathways could not be ruled out because Φ_r^S = 0.18 for the D. $FRET_{T\text{-}S}$ at 77 K has also been used to study the orientation of the D and A in the tetrameric enzyme yeast L-lactate dehydrogenase (cytochrome b).[47] Several biomolecule-based chromophores have also been experimentally tested for $FRET_{T\text{-}S}$ at low temperatures, in addition to $FRET_{S\text{-}S}$.[48-50] Another case of low-temperature $FRET_{T\text{-}S}$ in a polymer has been reported owing to the triplet impurity. The $FRET_{T\text{-}S}$ process occurred between the triplet state of the α,β-unsaturated carbonyl impurities in nylon-6,6 polymer and the doped A dye 3-methoxybenzanthrone (MBA) owing to the decreases of the phosphorescence intensity and lifetime of the polymer at 77 K with increasing MBA concentration.[51] For the triplet impurities, confusion about the chemical design of metal-free RTP, which is caused by triplet impurities, has been recently reported for crystalline conjugated molecular materials.[52-56] Clarifying the relationships among k_r^T, k_{nr}^T, k_q, and chemical structures is necessary to minimize the confusion and enable more accurate chemical design of chromophores for RTP. Recently, the prediction quality of k_r^T and k_{nr}^T using quantum chemical calculations for a variety of chemical structures has significantly improved, helping to obtain large Φ_r^T.[28] Φ_r^T is related to $R_{T\text{-}S}$ based on equation (6), and insight into k_r^T and k_{nr}^T using quantum chemical calculations may contribute to the development of novel D for $FRET_{T\text{-}S}$.

After observation of $FRET_{S\text{-}S}$ in chemiluminescence in the 1960s,[57] there was discussion about Dexter energy transfer and $FRET_{T\text{-}S}$ in chemiluminescence (c in Fig. 3). The possibility of $FRET_{T\text{-}S}$ for chemiluminescent 2,3-dihydrophthalazine-l,4-dione derivatives as the D to diphenylanthracene derivatives as the A unit has been discussed.[58] Although large enhancement of the chemiluminescence was observed from the change of the A from 9,10-diphenylanthracene to 9,10-dibromoanthrancene, the absorption spectra and ε_A values of the two As were the same. Therefore, the authors explained that Dexter-type energy transfer from the D to the A is related to the enhancement of the chemiluminescence. They also suggested the possibility of thermally activated fluorescence after triplet formation in 9,10-diphenylanthracene after Dexter-type energy transfer to explain the enhancement of the chemiluminescence.[58] Because k_q ($+k_{nr}^T$) becomes small compared with k_r^T at 77 K for heavy-atom-free Ds, Φ_r^T does not become 0 and the enhancement of Φ_r^T leads to large $R_{T\text{-}S}$ (Fig. 4d). Therefore, the window for $FRET_{T\text{-}S}$ is wider than that for Dexter energy transfer in which direct contact between the D and the A is required at 77 K. However, k_q ($+k_{nr}^T$) at RT becomes much larger than k_r^T at 77 K to induce chemiluminescence, resulting in $\Phi_r^T \approx 0$ at RT. For example, $R_{T\text{-}S}$ becomes approximately 1 nm or less when Φ_r^T = 0.001 at high temperature even when $J(\lambda)$ is large (Fig. 4e). In this situation, $FRET_{T\text{-}S}$ could occur at high temperature for R_{DA} to also allow Dexter-type energy transfer. Therefore, the separation or distinguishing Dexter-type energy transfer from the triplet state and $FRET_{T\text{-}S}$ at RT might be difficult because of the distance. After the report,[58] the possibility of $FRET_{T\text{-}S}$ from a chemiluminescent D to 9,10-dibromoanthrancene was discussed for a few years. However, separation of Dexter-type

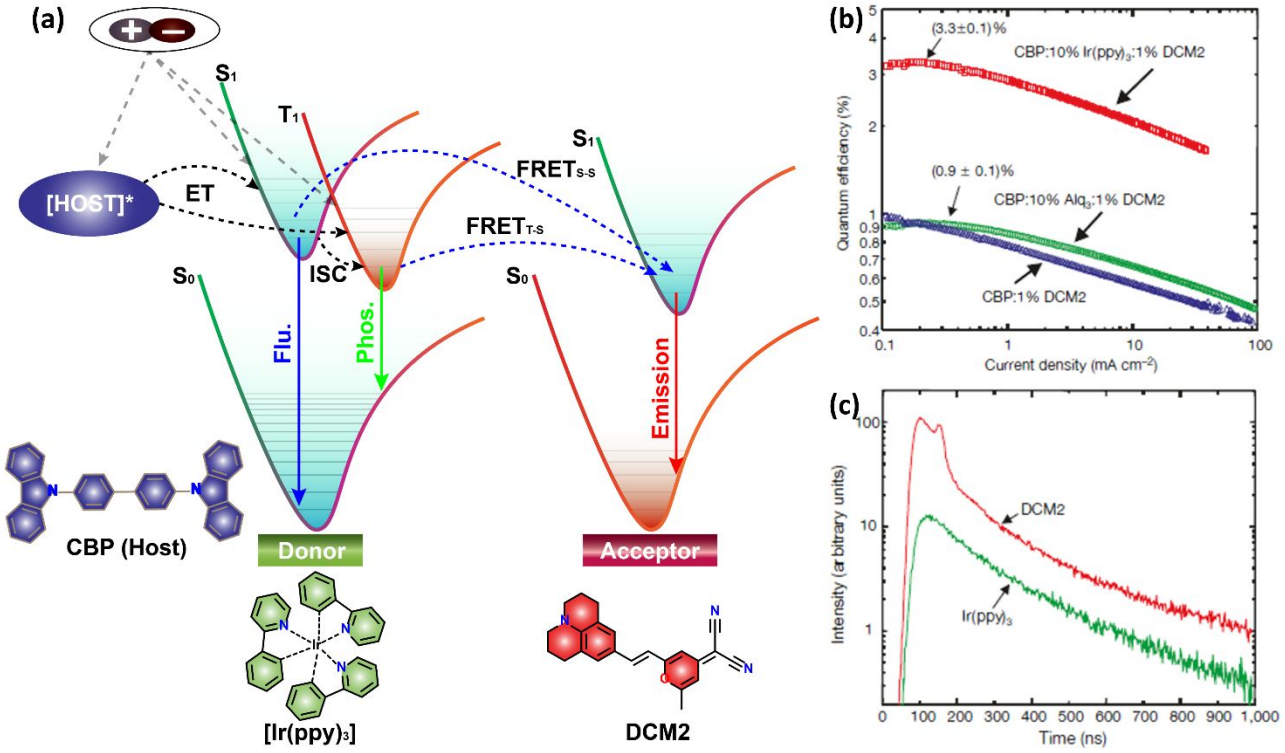

Fig. 5 (a) Schematic illustration of multi-step energy transfer from the host (CBP) to the organometallic phosphor [Ir(ppy)$_3$] to the fluorescent dye (DCM2) as the acceptor (emitter) in electroluminescence devices. Both FRET$_{S\text{-}S}$ and RT FRET$_{T\text{-}S}$ occurred from the phosphorescent sensitizer to the fluorescent dye. (b) External quantum efficiency versus current density plot of DCM2 based on three comparative devices. The emitting layers of devices were 1% DCM2 in CBP, 10% Alq$_3$ (sensitizer) and 1% DCM2 in CBP, and 10% Ir(ppy)$_3$ (sensitizer) and 1% DCM2 in CBP. (c) Transient decay profile of the DCM2 and Ir(ppy)$_3$ components in the device with 10% Ir(ppy)$_3$ and 1% DCM2 in CBP as an emitting layer. Reproduced with permission from Springer Nature.[3]

energy transfer and FRET$_{T\text{-}S}$ at high temperature to induce chemiluminescence has not been discussed.[59] Although discussion of the triplet decay change from the D in the absence and presence of the A and the phosphorescence yield of the D at high temperature might clarify FRET$_{T\text{-}S}$ at high temperature, these data have not been reported. Thus, clear FRET$_{T\text{-}S}$ at RT was not reported before 2000.

RT FRET$_{T\text{-}S}$ from organometallic donors

In the late 1990s, many phosphorescent emitters of heavy-metal complexes were developed and found to be suitable materials for optoelectronic devices owing to the high radiation rate from T_1 to S_0 at RT to allow nearly 100% RTP yield, indicating $\Phi_r^T \simeq 100\%$, and the internal quantum efficiency of electroluminescence devices could reach 100%.[60-62] Owing to the high k_r^T because of using heavy atoms for the organometallic D, $k_r^T > (k_{nr}^T + k_q)$, leading to $\Phi_r^T \simeq 100\%$. $k_r^T > (k_{nr}^T + k_q)$ allows rapid FRET$_{T\text{-}S}$ from the organometallic D to the fluorescent A (d in Fig. 3).

The longer triplet lifetime of organometallic RTP emitters compared with the lifetime of conventional fluorescent emitters triggers triplet-triplet annihilation at a high electro-excitation rate. This causes a decrease in the electroluminescence efficiency at high brightness in electroluminescence devices. To utilize the triplet exciton of organometallic-based phosphorescent dyes in electroluminescence devices, Baldo et al. successfully achieve triplet exciton harvesting of tris(2-phenylpyridinato)iridium(III) [Ir(ppy)$_3$] as a phosphorescent D to 4-(Dicyanomethylene)-2-methyl-6-(4-dimethylaminostyryl)-4*H*-pyran (DCM2) as a fluorescent A (DCM2) via FRET$_{T\text{-}S}$ in electroluminescence devices (Fig. 5a).[3] They fabricated a variety of electroluminescence devices using 10% Ir(ppy)$_3$ phosphorescence dye in the 4,4′-bis(N-carbazolyl)-1,1′-biphenyl (CBP) host and 1% fluorescent dye in the CBP host in alternating layers of the device. Higher external electroluminescence quantum efficiency (EQE) of 3.3% was achieved for the Ir(ppy)$_3$–DCM2 pair device compared with that for only DCM2 and the (tris(8-hydroxyquinolinato)aluminum) [Alq$_3$]-DCM2 pair device (EQE = 0.9%) (Fig. 5b). This indicates that there was no sensitized emission in the Alq$_3$–DCM2 pair. Furthermore, the transient decay kinetics of the Ir(ppy)$_3$–DCM2 pair were recorded using electrical pulse excitation (Fig. 5c). The decay lifetimes of DCM2 and Ir(ppy)$_3$ were ~1 and ~500 ns, respectively. The decay lifetime of the Ir(ppy)$_3$–DCM2 pair was ~100 ns, along with a hump for the short component (Fig. 5c). This indicates that both the singlet and triplet energies from the D [Ir(ppy)$_3$] were transferred to the fluorescent A (DCM2). The calculated FRET$_{T\text{-}S}$ efficiency based on the lifetime of the D in the absence and presence of the A was approximately 80%. Hence, the rapid FRET$_{T\text{-}S}$ from Ir(ppy)$_3$ to DCM2 and the subsequent rapid radiation from DCM2 reduced the device efficiency roll-off, leading to improvement of the device performance (Fig. 5b and 5c). Similarly, FRET$_{T\text{-}S}$ at RT has been demonstrated for red-emitting polymer light-emitting-diode devices.[3] Dual FRET$_{T\text{-}S}$ and FRET$_{S\text{-}S}$ from the green-emitting phosphorescent sensitizer iridium(III) bis(2-phenylpyridinato)acetylacetonate

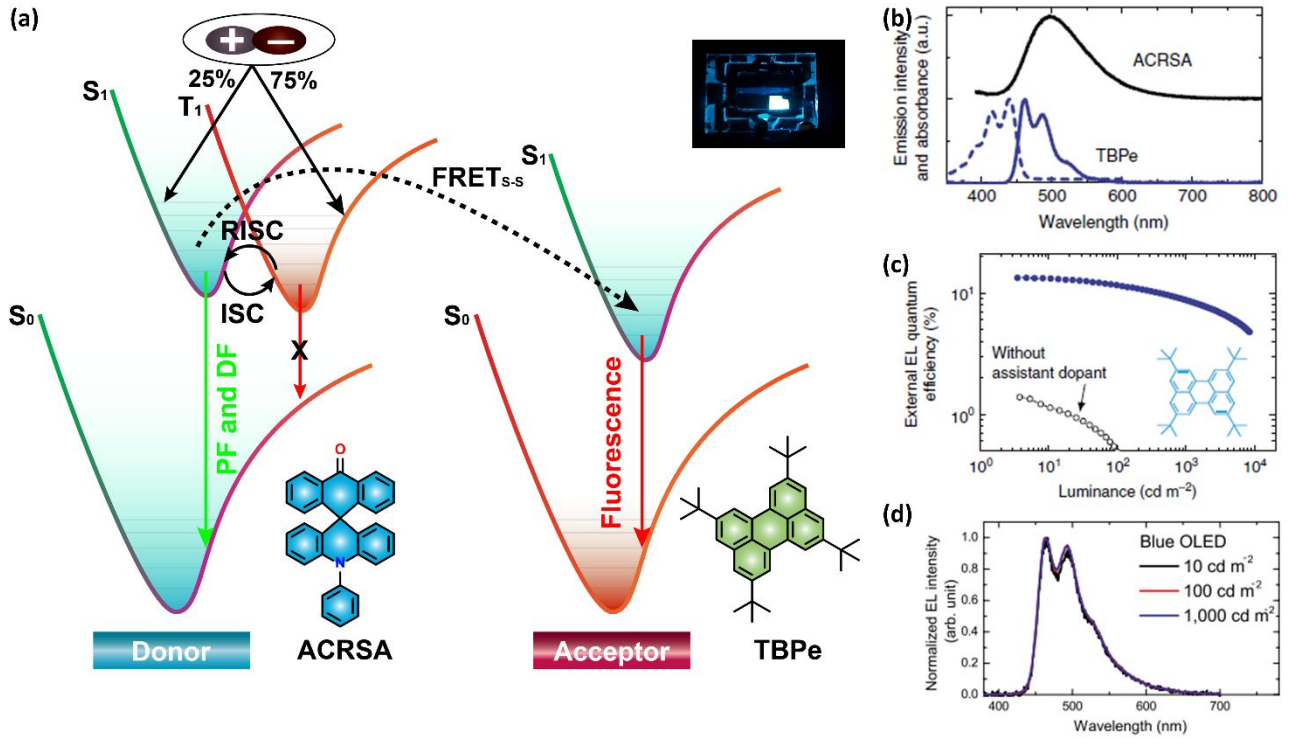

Fig. 6 $FRET_{S\text{-}S}$ in hyperfluorescence devices. (a) Jablonski energy profile diagram showing $FRET_{S\text{-}S}$ from a thermally activated delayed-fluorescence emitter (ACRSA) as the D to a fluorescent dye (TBPe) as the A. (b) Normalized emission spectrum of ACRSA, and the absorption and emission spectra of the TBPe A showing the spectral overlap for $FRET_{S\text{-}S}$. (c) and (d) Electroluminescence characteristics of the FRET pair devices showing the enhancement of the device performance. PF = prompt fluorescence, DF = delayed fluorescence. Reproduced with permission from Springer Nature.[4]

$[Ir(ppy)_2(acac)]$ (1%) to the fluorescent dye Nile red (1%) of the single-layer polymer device exhibited 6.5 cd/A. This shows the potential of application of electronically generated triplet exciton for harvesting via FRET to a fluorescent dye in electroluminescence devices.

$FRET_{S\text{-}S}$ from the triplet state via RISC

From the spin statistics, the efficiency of pure organic chromophores in electroluminescence devices is limited to 25%. This is because 75% of the triplet excitation cannot be used owing to either no radiation from T_1 or the long lifetime of heavy-metal-free chromophores.[63] For thermally activated delayed fluorescence (TADF), 75% of the triplet excitons can be harvested via thermally activated RISC to the singlet state followed by emission from the lowest singlet state, which is known as a scheme to efficiently extract emission from heavy-metal-free molecules.[64] Several molecular design principles to enhance the RISC rate (k_{risc}) have recently been reported, leading to high device performance in blue, green, and red electroluminescence devices.[65] However, these molecules are mainly D–A-based charge-transfer chromophores. The broad emission bands and low quantum yield in the lower energy levels are the major issues that limit the color purity and efficiency of the device in the red/near-infrared (NIR) region, respectively.

To address this issue, Nakanotani et al. demonstrated $FRET_{S\text{-}S}$ from a TADF emitter as the D to a fluorescent A in an electroluminescence device (e in Fig. 3). Variation of different color TADF emitters as the Ds in combination with the As achieved highly efficient organic light-emitting diodes (OLEDs) with EQE of 13.5%, 15.8%, 18%, and 17.5% for blue, green, yellow, and red, respectively.[4] The Jablonski diagram showing the electronically excited S_1 and T_1 of the TADF molecule 10-phenyl-10*H*,10′*H*-spiro[acridine-9,9′-anthracen]-10′-one (ACRSA) as the D with RISC between S_1 and T_1 is shown in Fig. 6a. The electro-generated T_1 exciton was harvested via the RISC process to S_1 and subsequent $FRET_{S\text{-}S}$, leading to emission from blue-emitting 2,5,8,11-tetra-*tert*-butylperylene (TBPe) as the A (Fig. 6a). Owing to the spectral overlap between the absorption spectrum of TBPe and the emission spectrum of ACRSA, the singlet exciton energies of the D were resonantly transferred to the singlet states of the A, leading to emission from TBPe (Fig. 6b). As a result, an electroluminescence device based on the ACRSA (15 wt%)–TBPe (1 wt%) pair exhibited better EQE(max) of 13.4% in the blue device (CIE = 0.17, 0.30) with reduced device roll-off at high luminance (Fig. 6c). This is known as a hyperfluorescence device. Another benefit of using this process is the increase in the color purity of the electroluminescence for full-color displays. For TADF chromophores, the fluorescence spectrum often becomes broad because of the strong charge-transfer nature of the fluorescence. However, a fluorescent A can be used with chromophores with a strong local excited nature in fluorescence. Indeed, the vibrational electroluminescence spectrum indicated many contributions of the fluorescent A with a local excited nature (Fig. 6d). However, $FRET_{T\text{-}S}$ is a competitive pathway for $FRET_{S\text{-}S}$. To selectively harvest the triplet excitation via $FRET_{S\text{-}S}$ in hyperfluorescence devices, there should not be any $FRET_{T\text{-}S}$. Hence, k_{risc} should be very high at RT ($>10^6$ s^{-1}) compared with the small k_r^T of heavy-

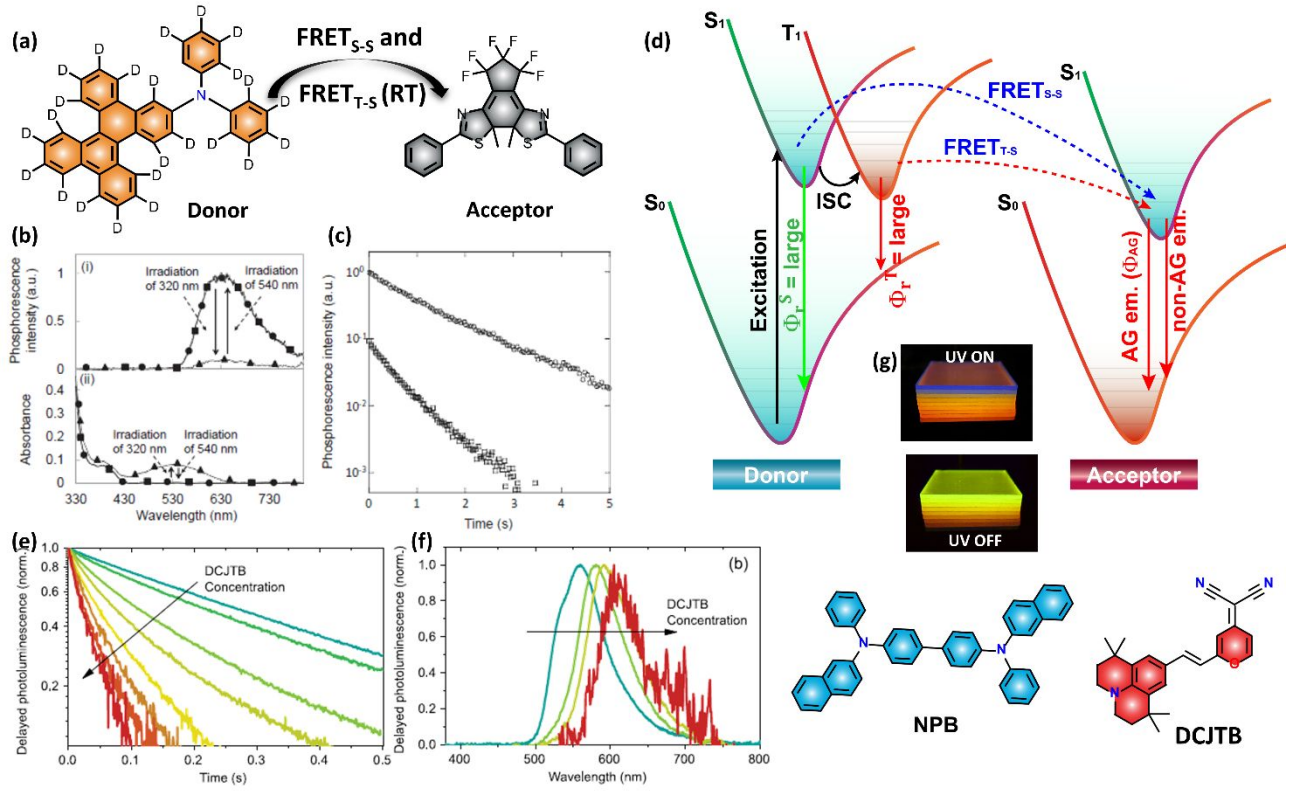

Fig. 7 Dual FRET$_{S-S}$ and FRET$_{T-S}$ from purely organic phosphorescent materials at RT. (a) Molecular structure of the phosphorescent D and closed form of the photochromic diarylethene derivative as the A used to show FRET$_{T-S}$ from the D to the A in the amorphous *β*-estradiol host at RT under ambient conditions. (b) Reversible (i) persistent RTP intensity changes and (ii) absorbance changes depending on UV and green light irradiation for the film of the material in (a). (c) RTP decay characteristics of the RTP (open circles) and non-RTP (open squares) states in air. The decrease in the RTP lifetime of the D with the change from the absence of A (open circles) before UV irradiation to the presence of A (open squares) after UV excitation indicates RT FRET$_{T-S}$ from the D to the A. Reproduced with permission from Wiley VCH.[70] (d) Jablonski diagram showing prompt and delayed afterglow fluorescence from the A after dual FRET$_{S-S}$ and FRET$_{T-S}$ from NPB as a D to DCJTB as a fluorescent A at RT. (e) and (f) Afterglow emission spectra and decay profiles with variation of the concentration of the A, respectively. (g) Digital photographs showing the red afterglow emission from the DCJTB A when the UV light was turned off. Reproduced with permission from the American Chemical Society.[72]

atom-free chromophores. Dexter energy transfer from the T_1 of a heavy-atom-free D to the T_1 of a fluorescent A results in T_1 generation of the A. Because this results in no emissive extraction and/or no rapid emission, carefully choosing the concentration and good dispersion of the fluorescent A are crucial to enhance the EQE.

Dual FRET$_{S-S}$ and FRET$_{T-S}$ from organic chromophores at RT

Many simple heavy-atom-free chromophores with Φ_{ISC} > 50% were reported in the twentieth century.[66] However, phosphorescence from heavy-atom-free chromophores often requires a very low temperature and Φ_r^T often becomes 0 at RT. Detailed analysis of triplet quenching at RT has been reported in the last 10 years, and the origin of thermally activated triplet quenching at RT is gradually becoming understood.[26,28] In many cases, Φ_r^T = 0 at RT is often caused by k_q even under high vacuum conditions. However, the use of an appropriate host to allow triplet confinement using deep trapping of T_1 of heavy-atom-free chromophores greatly decreases k_q at RT, allowing the occurrence of a certain amount of RTP, mainly depending on k_r^T and k_{nr}^T of the chromophore.[33,34] Because of the much-suppressed k_q at RT, k_r^T often has comparable magnitude to k_q. Because $k_{\mathrm{FRET}_{T-S}}$ is proportional to k_r^T, $k_{\mathrm{FRET}_{T-S}}$ also often increases more than k_q at RT. The comparable magnitudes of $k_{\mathrm{FRET}_{T-S}}$ and k_q because of the suppressed k_q clearly opens the door for the possibility for FRET$_{T-S}$ in addition to FRET$_{S-S}$ from heavy-atom-free Ds at RT under ambient conditions (f in Fig. 3).

The possibility of RT FRET$_{T-S}$ from 3,6-bis(5-methoxyindol-1-yl)-9-(4-methoxyphenyl)carbazole (BIPC3) as the D to a fluorescent A has been reported in OLED research.[67] Experimentally, RT delays emission from the A, with at least 30 μs delay time indicating the possibility of RT FRET$_{T-S}$. However, the calculated energy difference between S_1 and T_1 of BIPC3 and the fluorescent A is small. This suggests the possibility of TADF at RT, because it has often been considered in the last 10 years.[64,65] Because the delayed emission decay characteristics and spectra are often measured, consideration of the possibility of TADF and/or FRET$_{S-S}$ using TADF of the D may be important from an experimental viewpoint. For a logical viewpoint, $k_{\mathrm{FRET}_{T-S}}$ approaching 10^6 s^{-1} is relatively large for BIPC3 as a heavy-atom-free D. Because the magnitude of k_r^T, which is proportional to $k_{\mathrm{FRET}_{T-S}}$, has recently been well predicted by quantum calculations,[28,32,68] screening of k_r^T of BIPC3 and the fluorescent A will assist in a clear understanding of this point.

Clear RT FRET$_{T-S}$, in addition to FRET$_{S-S}$, from a heavy-atom-free D was reported by Katsurada et al. with a distinct change of the afterglow (lifetime of more than 100 ms) RTP decay of the D in the presence and absence of an A.[69] Amorphous β-estradiol doped with deuterated 3-

(diphenylamino)dibenzo[g,p]chrysene (DPA-DBC) was used as the D and photochromic diarylethene derivatives were used as the A. For the D, owing to suppression of k_q at RT in amorphous β-estradiol, $k_{nr}^T + k_q$ at RT largely decreases and approximately becomes 10 times compared with the small value of k_r^T. This allowed red persistent RTP with a yield of 5.3% and a lifetime of 1.12 s at RT (Fig. 7a). k_r^T, k_{nr}^T, and k_q leading to Φ_r^T of DPA-DBC as the D have been analyzed from experimental and theoretical viewpoints.[70] The values of small k_r^T and Φ_r^T reasonably well explained the small magnitude of $k_{FRET_{T-S}}$ and possible RT $FRET_{T-S}$ from the D. Because no spectral overlap between the phosphorescence spectrum of the D and the absorption spectrum of the open form of the A was observed, there was no noticeable FRET from the D to the A to cause the large persistent RTP yield (circles in Fig. 7b). However, after ultraviolet (UV) irradiation, the closed isomer of A formed. The closed isomer of A showed absorption spectrum overlap with the fluorescence and phosphorescence spectra of D. The occurrence of spectral overlap, in addition to a certain value of Φ_r^T at RT for D, triggered RT $FRET_{T-S}$, in addition to $FRET_{S-S}$, resulting in a large decrease of the RTP yield (triangles in Fig. 7b). The additional $FRET_{T-S}$ from the D in the presence of the closed form of A was confirmed by the decrease of the RTP lifetime (Fig. 7c). The RTP yield was recovered by transforming the closed form of A to the open form of A after irradiation with green light (squares in Fig. 7b). Emission color tuning using RT $FRET_{T-S}$ from heavy-atom-containing chromophores and heavy-atom-free chromophores as the D to a fluorescent A was then reported, and it has been used for biological analysis.[71] The RTP lifetime of the D in the absence of the fluorescent A had a magnitude of 100 μs. The existence of RT $FRET_{T-S}$ was confirmed by the decrease of the RTP decay in the presence of the fluorescent A. However, longer lifetime is generally recommended for time-resolved imaging using two-dimensional and cost-effective photodetectors.

Afterglow color change by dual $FRET_{S-S}$ and $FRET_{T-S}$ at RT (g in Fig. 3) using a RTP emitter (*N*,*N*-di(naphtha-1-yl)-*N*,*N*-diphenylbenzidine [NPB]) as the D and 2-*tert*-Butyl-4-(dicyanomethylene)-6-[2-(1,1,7,7-tetramethyljulolidin-9-yl)vinyl]-4*H*-pyran (DCJTB) as the red fluorescent A was first reported by Kirch et al. (Fig. 7d).[72] The NPB chromophore doped in a poly(methyl methacrylate) matrix showed Φ_r^S = 28%, Φ_{AG} = 3%, τ_f = 1.8 ns, and τ_{AG} = 364 ms at RT, where Φ_{AG} is the afterglow RT emission yield, τ_f is the fluorescence lifetime, and τ_{AG} is the average lifetime of afterglow RT emission. In the presence of different weight percentages of DCJTB as the A, the fluorescence lifetime, as well as the afterglow lifetime, of 2 wt% NPB significantly decreased. τ_f (1.8 ns) decreased to τ_f = 0.105 ns in the presence of 1.4 wt% of the DCJTB acceptor. Similarly, τ_{AG} (364 ms) of the D decreased to τ_{AG} = 75 ms in the presence of 1.4 wt% of the A (Fig. 7e). With increasing concentration of the DCJTB acceptor, the afterglow emission color red-shifted (Fig. 7f). Consequently, red afterglow emission from the D was obtained. This was because of the good correlation between the estimated R_{S-S} of 3.7 nm and the approximated R_{T-S} of 2.6 nm assuming $\Phi_r^T = \Phi_P$ using the lifetime measurement results, indicating significant $FRET_{T-S}$ rather than Dexter-type energy transfer. The dual $FRET_{S-S}$ and RT $FRET_{T-S}$ from the D to the fluorescent A resulted in an afterglow RT emission color change. After reports of representative examples,[72,73] the afterglow color change using the dual $FRET_{S-S}$ and RT $FRET_{T-S}$ from the several organic D owing to suppressed k_q and/or k_{nr} along with radiation from the singlet state have been reported (h in Fig. 3).

For afterglow color changes, it should be noted that Dexter energy transfer and the rapid delayed fluorescence after Dexter energy transfer are not logically related to generation of the afterglow process. This is because the Dexter energy-transfer process with direct molecular orbital overlap is a rapid process, which precludes a long delay of the excitons to allow afterglow. However, if a solid doped with only A in the absence of a D exhibits afterglow-delayed RT fluorescence via slow RISC[74] and triplet-triplet annihilation,[75] afterglow emission via Dexter energy transfer is logically possible. This is because a long delay occurs in the slow RISC process and triplet-triplet annihilation in the A. Experiments using solids doped with only an A in the absence of a D can clarify if the afterglow is caused by the afterglow emission based on delayed fluorescence via slow RISC and triplet-triplet annihilation.

Selective RT $FRET_{T-S}$ from organic chromophores

Although dual $FRET_{S-S}$ and $FRET_{T-S}$ at RT to change the afterglow color to longer wavelength has been reported, a rapid fluorescent A caused by $FRET_{S-S}$ from D to A does not contribute to afterglow RT emission imaging independent of the autofluorescence using cost-effective and small-scale detectors. Therefore, a concept to allow large suppression of $FRET_{S-S}$ with large enhancement of RT $FRET_{T-S}$ could be crucial (i in Fig. 3).

Recently, Sk et al. reported selective and efficient $FRET_{T-S}$ at RT from the N-fused chromophore (dibenzo[a,c] phenazine-d_{12} [DBPz-d_{12}] as the D to the red-emitting dye DBP as the A in an appropriate solid host (Fig. 8a).[76] To enhance $FRET_{T-S}$, it is recommended to use a D with large Φ_r^T. One way to enhance k_r^T without an increase of ($k_{nr}^T + k_q$) and achieve larger Φ_r^T is to use a large transition dipole moment from the singlet states (Fig. 2f). However, this often facilitates k_r^S and Φ_r^S, which enhances $FRET_{S-S}$ as an afterglow-deactivation pathway.[77] The out-of-plane distortions in the molecular vibrations of DBPz-d_{12} molecules containing heteroatoms in the fused ring play a role in the increase of k_r^T without increasing k_{nr}^T (A in Fig. 8b), which increases Φ_r^T to 0.21 at RT (B in Fig. 8b). In addition, the out-of-plane distortion enhances Φ_r^T without the increase of Φ_r^S because the vibration inducing the distortion is not related to k_r^S and cannot increase Φ_r^S. Moreover, the different ππ* character in the S_1–S_0 transition and nπ* character in the T_2–S_0 transition facilitate k_{isc} from S_1 based on the El-Sayed rule (C in Fig. 8b).[78] Therefore, nearly zero Φ_r^S is obtained for the DBPz-d_{12}, minimizing $FRET_{S-S}$.

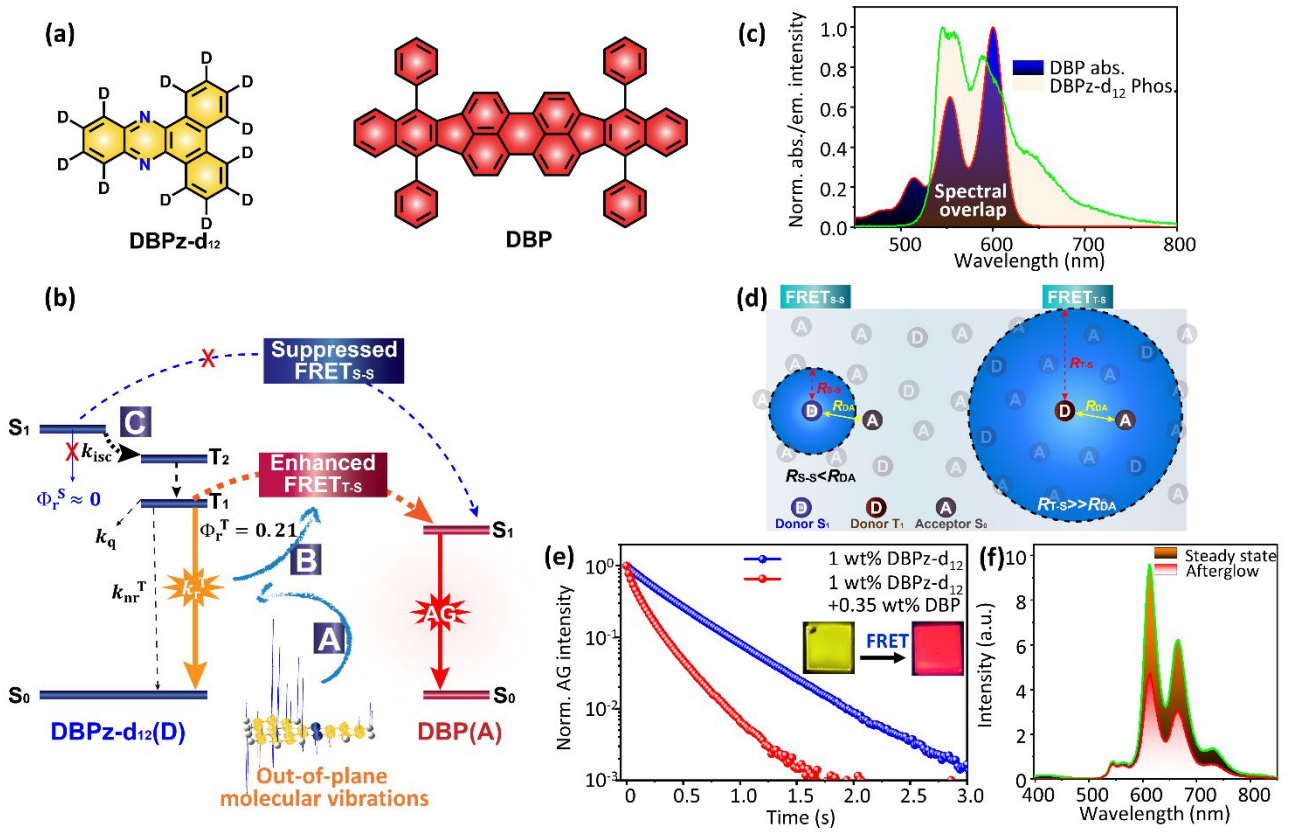

Fig. 8 Selective and efficient $FRET_{T\text{-}S}$ for long-wavelength afterglow emission at RT. (a) Molecular structure of the N-fused chromophore DBPz-d_{12} as the D and red fluorescent DBP as the A. (b) Jablonski diagram showing selective RT $FRET_{T\text{-}S}$, as well as suppressed $FRET_{S\text{-}S}$. (c) Spectral overlap between the normalized phosphorescence spectrum of 1-wt% DBPz-d_{12} and the absorption spectrum of 0.1-wt% DBP in an amorphous 2,8-bis(diphenyl-phosphoryl)-dibenzo[*b,d*]thiophene (PPT) host at RT. (d) Relationships among $R_{T\text{-}S}$, $R_{S\text{-}S}$, and R_{DA}. (e) Afterglow RT emission decay of a PPT film doped with DBPz-d_{12} in the absence and presence of 0.35-wt% DBP. (f) Steady-state and afterglow RT emission spectra at 380 nm-excitation of an amorphous PPT film doped with 1-wt% DBPz-d_{12} and 0.35-wt% DBP. Reproduced with permission from Wiley VCH 2022.[76]

The compatibility of the enhanced Φ_r^T and near-zero Φ_r^S allows selective and efficient $FRET_{T\text{-}S}$ from a heavy-atom-free D to a fluorescent A at RT. DBP was selected as the fluorescent A because of the large spectral overlap between the absorption spectrum of DPB and the phosphorescence spectrum of DBPz-d_{12} (Fig. 8c). At RT, the large Φ_r^T significantly contributed to the increase in $R_{T\text{-}S}$ to 4.3 nm because $R_{T\text{-}S}$ is proportional to $(\Phi_r^T)^{1/6}$ based on equation (6). In contrast, the near-zero Φ_r^S considerably decreased the $R_{S\text{-}S}$ to 1.5 nm. Because $R_{D\text{-}A}$ was estimated to be 2.0 nm when the acceptor concentration was 0.35 wt%, the many DBP acceptors located within the large $R_{T\text{-}S}$ enabled efficient $FRET_{T\text{-}S}$ (right-hand part of Fig. 8d). Therefore, the decrease of the RTP lifetime of DBPz-d_{12} in the presence of 0.35 wt% of the DBP A showed distinct RT $FRET_{T\text{-}S}$ (Fig. 8e). However, $FRET_{S\text{-}S}$ was infrequent because most of the DBP As were located outside the small $R_{S\text{-}S}$ (left-hand part of Fig. 8d). Therefore, selective and efficient $FRET_{T\text{-}S}$ resulted in RT red afterglow emission from the DBP A with a yield of 17% (Fig. 8f).

Recent progress in RT FRET involving the triplet state from the viewpoint of applications

$FRET_{S\text{-}S}$ has been extensively applied as a spectroscopic ruler in biomedical imaging and sensing to calculate the distance between two terminals. In addition, $FRET_{S\text{-}S}$ via RISC from a TADF sensitizer to a fluorescent dye is promising for application in display devices. This is because the fast k_{risc} leads to enhancement of the device performance, color purity, and longer wavelength emission. For example, Chan et al. reported a pure-blue (CIE = 0.13, 0.16, FWHM = 19 nm) electroluminescence device with high efficiency of 32% at 1000 cd m^{-2} (EQE_{max} = 41%) and good stability (Fig. 9a).[79] The fast k_{risc} (8.6×10^5 s^{-1}) of the TADF sensitizer (HDT-1) as a D led to rapid $FRET_{S\text{-}S}$ to the fluorescent A (*v*-DABNA) for better color purity and higher device performance compared with the sensitizer- and emitter-dye-only devices (Fig. 9a(ii)). Similarly, Cui et al. reported large k_{risc} (1.5×10^7 s^{-1}) to harvest the triplet excitons in a D–A type (5Cz-TRZ) molecule by incorporating multiple D units on the A core to form the charge-resonance-type hybrid triplet state (Fig. 9b). This facilitated efficient $FRET_{S\text{-}S}$ to the assistant dopants (Fig. 9b(i)).[80] As a result, longer operational lifetime of the device, along with comparable device performance (EQE = 24%, device D, sky blue), was obtained (Fig. 9b(ii)). However, slightly lower EQE and efficiency roll-off were obtained, which may be because of hole trapping by the fluorescent dye. Cascade $FRET_{S\text{-}S}$ from a blue TADF sensitizer to green and red fluorescent dyes as assistant dopants has been found to be suitable for white OLEDs.[81] Shahalizad et al. reported triplet harvesting via $FRET_{S\text{-}S}$ in electroluminescence devices to obtain a NIR emissive device containing a TADF

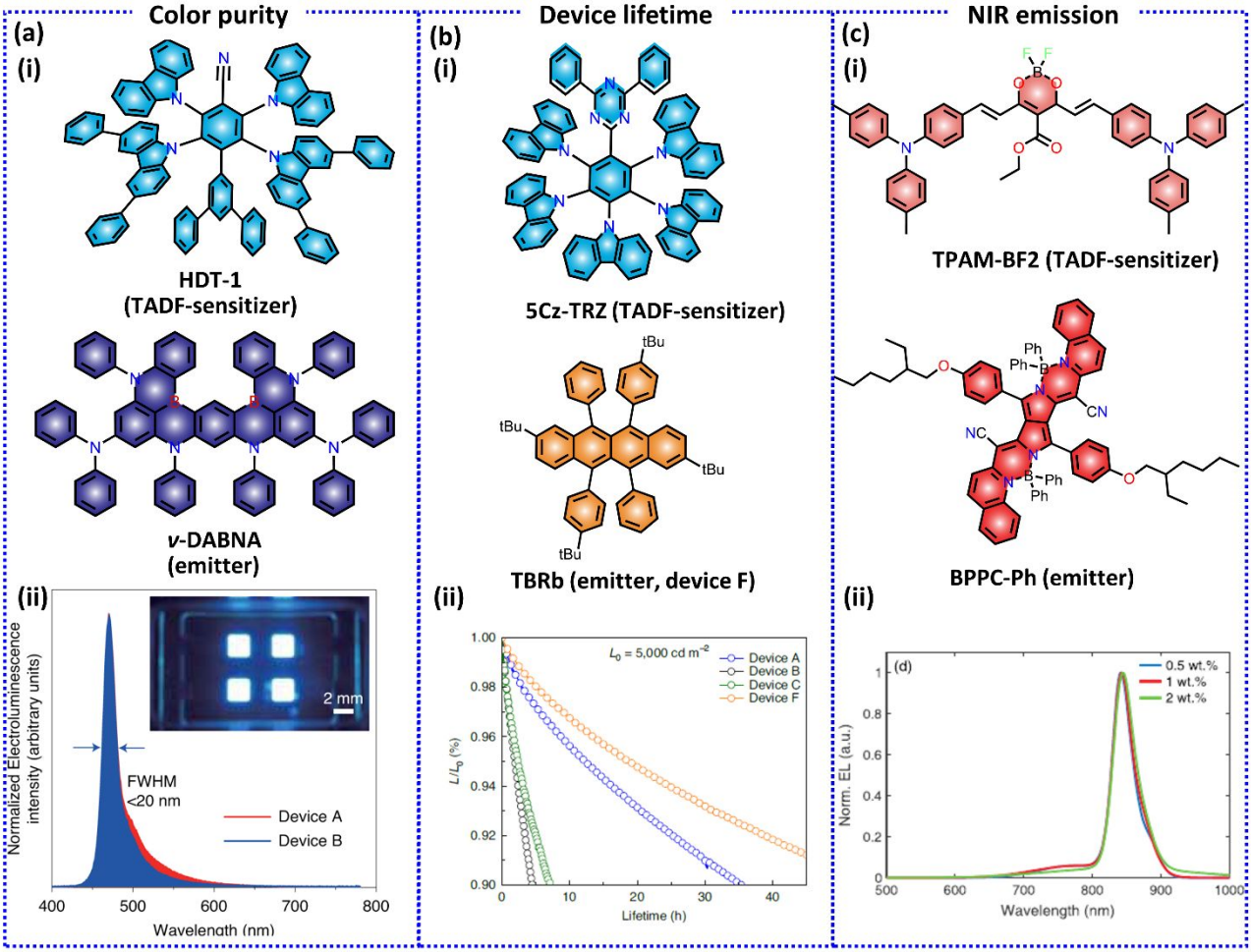

Fig. 9 Benefits of $FRET_{S\text{-}S}$ via RISC for the (a) color purity, (b) device operating lifetime, and (c) highly efficient NIR electroluminescence devices. The chemical structures of the TADF sensitizers as the D and the fluorescent dyes as the A are shown in (i). The characteristics of the electroluminescence spectra from films containing TADF sensitizer as a D and emitter as an A (a and c) and the device operational lifetimes of the TADF emitter only devices (device A-C) and D-A pair device containing 5Cz-TRZ as the TADF sensitizer (D) and TBRb as the A (device F) (b) are shown in (ii). (a) is reproduced with permission from Springer Nature.[79] (b) is reproduced with permission from Springer Nature.[80] (c) is reproduced with permission from Wiley VCH.[82]

sensitizer (TPAM-BF2, 20%) with a NIR-emitting fluorescent dye (BPPC-Ph, 0.5%) exhibiting EQE(max) of up to 3.5% at 840 nm with color purity (FWHM < 40 nm) (Fig. 9c).[82] Therefore, $FRET_{S\text{-}S}$ via RISC is promising for optoelectronic applications of heavy-metal-free devices to efficiently harvest 75% of the triplet excitons.

In the same way, the delayed emission from the A after RT $FRET_{T\text{-}S}$ has recently been considered to be a candidate for time-resolved emission imaging. For example, Dai et al. reported that the aqueous medium delayed fluorescence in the NIR region at 680 nm with a lifetime of 64 μs from an A (Nile Blue [NiB]) based on confinement of the RTP chromophore (G) loaded in β-cyclodextrin-grafted hyaluronic acid (HACD) in the cucurbit[7]uril (CB[7]) cavity (G□CB[7] @ HACD) (Fig. 10a–c).[12] RT $FRET_{T\text{-}S}$ was observed owing to the considerable spectral overlap between the phosphorescence spectrum of G and the absorption spectrum of NiB. The lifetime of the D (G) at 540 nm decreased from 0.581 to 0.385 ms in the presence of the A (NiB) (Fig. 10d), confirming the existence of RT $FRET_{T\text{-}S}$. The RT $FRET_{T\text{-}S}$ efficiency was 34%. The benefit of the NIR-delayed fluorescence in the aqueous medium with good biocompatibility was used for cancer-cell imaging. The cellular images of A549 (Fig. 10e) and HeLa (Fig. 10f) cancer cells in the NIR channel showed the bright-red signal of the cytoplasm distributed around the nucleus (DAPI channel). Similarly, another study demonstrated confinement in an aqueous medium using composite mesoporous silica nanoparticles (MSNs).[83] Encapsulating green phosphorescent ($BrBP\text{-}NH_2$) as an energy D and a red fluorescent A (rhodamine B or SR101) in MSNs led to red delayed fluorescence from the A. The decrease in the lifetime of the D with increasing concentration of the A indicated RT $FRET_{T\text{-}S}$. Owing to inefficient energy transfer, dual delayed emission (green from the D and red from the A) was obtained and investigated for distinguishing the false signals in HeLa cells. This type of long-wavelength delayed emission is useful for time-resolved emission imaging independent of the autofluorescence by using expensive gated detecting systems. When time-resolved emission imaging requires more cost-effective and small-scale two-dimensional photodetectors, such as general complementary metal-oxide-semiconductor and charge-coupled devices, afterglow quality of >~100 ms is recommended.[84] To obtain brightness of the afterglow from small-scale materials, short afterglow is also important. However, the long afterglow-delayed fluorescence after the

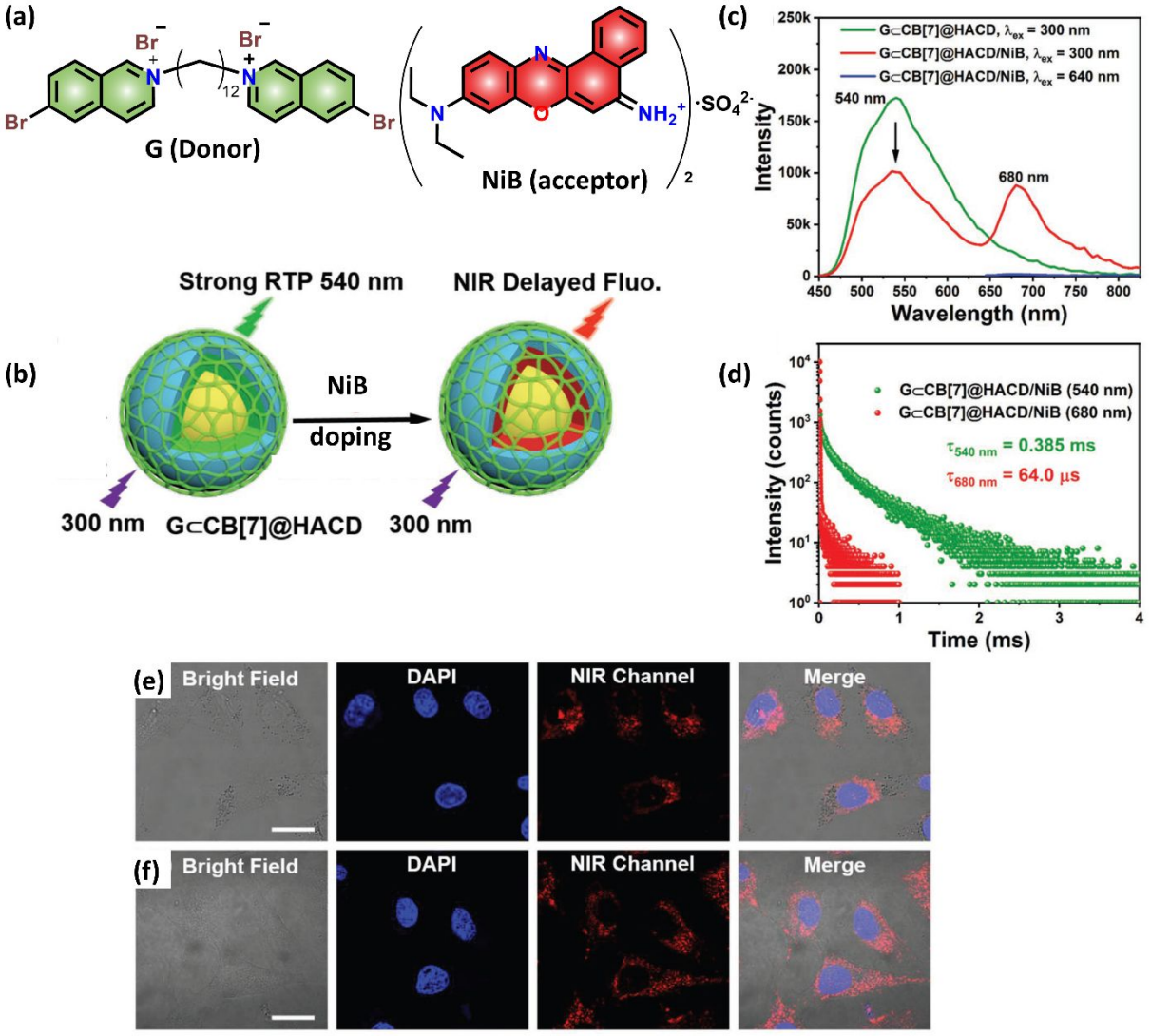

Fig. 10 (a) Molecular structure of the D generating RTP (G) and the A (NiB). (b) Schematic illustration of confinement of G loaded in β-cyclodextrin-grafted hyaluronic acid (HACD) in the cucurbit[7]uril (CB[7]) cavity (G⊂CB[7]@HACD) and loading of NiB. (c) RTP spectra of G⊂CB[7]@HACD under excitation at 300 nm (without A), G⊂CB[7]@HACD/NiB under excitation at 300 nm (with A), and G⊂CB[7]@HACD/NiB under excitation at 640 nm (with A) in water. (d) Emission decay profiles of G⊂CB[7]@HACD/NiB (with A) under excitation at 540 and 680 nm in water at 298 K. (e) Cellular images of A549 cancer cells. (f) HeLa cancer cells co-stained with the G⊂CB[7]@HACD/NiB assembly ([G] = 1.0×10^{-5} M, [CB[7]] = 3.0×10^{-5} M, [HACD] = 0.32 mg mL^{-1}, [NiB] = 6.0×10^{-7} M). Reproduced with permission from Wiley VCH.[12]

charge separation state[85,86] has sometimes been explained as phosphorescence. When this is applied to induce afterglow RT emission from an A after energy transfer, the $FRET_{S\text{-}S}$ caused by the delayed fluorescence from the D after charge separation triggers afterglow emission from the A. Because the controlled key parts in the D will be greatly different, careful consideration is crucial to guide precise design of the D.

FRET-based down conversion is an easy way to tune the afterglow emission color. Recently, RT $FRET_{T\text{-}S}$ from Ds with long-lived triplets to obtain full-color afterglow emission, including white light, for imaging or security printing applications has been investigated.[13,87,88] The RTP emitter was chosen as a sensitizer combined with a fluorescent dye to satisfy the criteria for energy transfer. For example, indolocarbazole isomers doped in a poly(vinyl alcohol) matrix exhibited strong cyan RTP emission (Φ_P = 5%–44%) with a long lifetime (0.38–2.04 s).[89] In combination with the fluorescent dye, the afterglow emission color was tuned from cyan to green to red, and the potential for anti-counterfeiting applications was demonstrated. Another paper reported intramolecular RT $FRET_{T\text{-}S}$ in a copolymer containing an afterglow host and a narrowband A core, leading to narrowband afterglow emission from the A core via RT $FRET_{T\text{-}S}$.[90] This material was further used as a photo-excited afterglow emitters on a top of general UV-light-emitting diodes to show afterglow patterns. Stimuli-responsive switching of the afterglow emission color has also been recently reported.[91,92] Hence, a variety of afterglow RT emission colors can be obtained from an A via RT $FRET_{T\text{-}S}$, which shows potential for imaging and anti-counterfeiting applications.

Summary and outlook

This feature article summarizes FRET involving triplet excited states from a logical perspective from the viewpoint of the D to the key developments for application of FRET in diverse fields, including optoelectronics, background-free imaging, and

sensing. The progress of FRET has inspired great recent interest in RT FRET involving triplet states, especially for light-emitting devices and time-resolved-imaging applications.

In FRET involving triplet states, our group's research has contributed to the following important aspects of RT $FRET_{T\text{-}S}$ from heavy-atom-free chromophores. Generally, the large k_q of materials at RT under ambient conditions precludes the possibility of RT $FRET_{T\text{-}S}$ from the D under ambient conditions, and no significant evidence for RT $FRET_{T\text{-}S}$ from Ds was reported. In 2013, our group reported that large triplet confinement of chromophores using host material with strong intermolecular interactions between the guest chromophore and the host largely decreases k_q, even in ambient conditions.[33] This enabled the design of materials that exhibit $FRET_{T\text{-}S}$ at RT, which was the first contribution of our group. The second contribution of our group was demonstration of $FRET_{T\text{-}S}$ from a heavy-atom-free D at RT under ambient conditions.[69] By using an appropriate host to allow large suppression of k_q, the changes of the RTP decay characteristics of a D in the presence and absence of an A depending on reversible isomerization of the photochromic A was demonstrated as proof of RT $FRET_{T\text{-}S}$ under ambient conditions. RT $FRET_{T\text{-}S}$ of an afterglow RT emitting D has recently been used for afterglow color tuning, even in materials. Because of the large suppression of k_q, $FRET_{T\text{-}S}$ is possible when the A concentration of the material increases to induce small R_{DA} for recently reported D–A pairs. However, the short R_{DA} because of the high concentration of the A also induces efficient $FRET_{S\text{-}S}$ as a negative deactivation pathway of afterglow emission. By using the original calculation procedures to enhance Φ_r^T at RT, the third contribution of our group was selective and efficient $FRET_{T\text{-}S}$ to overcome the above problem.[76] The molecular distortion effect using a conjugated backbone containing heteroatoms as the D to selectively enhance k_r^T without facilitating k_r^S allows selective and efficient $FRET_{T\text{-}S}$ from the D. It should be noted that the concept of selective $FRET_{T\text{-}S}$ logically allows efficient delayed emission from an A with relatively long emission wavelength because long-wavelength emitters often also contain large amounts of $\varepsilon_A(\lambda)$ in the visible wavelength. In the study, $R_{T\text{-}S}$ at RT was carefully determined using Φ_r^T at RT without any assumptions by measuring Φ_{ISC} for the first time, which was the fourth contribution from our group.[76] Thus, a platform to discuss the capability of an afterglow sensitizer as the D could be obtained through investigation from the viewpoint of the D. Through introduction of the chemical structures of the D–A pair and a general explanation of ε_A and the spectral overlap between the emission of the D and the absorption of the A, the knowledge obtained through the detailed research regarding RT $FRET_{T\text{-}S}$ from heavy-atom-free chromophores inspired us to provide an overview of FRET involving triplet states from the viewpoint of the D in this feature article.

The viewpoint from the D provides the following outlook for FRET involving triplet states. For RT $FRET_{S\text{-}S}$ from RISC, chemical design of the D with the combination of large ϕ_r^S and large k_{risc} is ideal for allowing compatibility between large EQE and small roll-off in high current density to allow more brightness in light-source applications. A large amount of doping of the A to induce more efficient $FRET_{S\text{-}S}$ is not recommend because significant introduction of the A increases the possibility of direct carrier trapping and/or triplet formation in the A, in addition to Dexter energy transfer from the D to the A to produce triplets in the A. Because a TADF D with large $R_{S\text{-}S}$ allows efficient $FRET_{S\text{-}S}$ using lower concentration of the A, chemical design of a TADF D with large ϕ_r^S and large k_{risc} to give large $R_{S\text{-}S}$ may be important. Because the device operational lifetime depending on different TADF Ds has recently been reported, chemical design of an appropriate D is also crucial for realistic applications. For RT $FRET_{T\text{-}S}$ from heavy-atom-free Ds for time-resolved imaging, including afterglow imaging, procedures to quantify $FRET_{T\text{-}S}$ need more careful treatment before considering chemical design of the D for RT $FRET_{T\text{-}S}$. For instance, because R_{DA} for the D and A is dispersed in the solid host, some D–A pairs with very small R_{DA} allow relatively rapid $FRET_{T\text{-}S}$ ($>10^3$ s^{-1}), while other D-A pairs with moderate R_{DA} result in slow $FRET_{T\text{-}S}$ ($<10^0$ s^{-1}). For decay measurements, only the longer components in the presence and absence of the A are often discussed for RT $FRET_{T\text{-}S}$, but this results in inaccurate estimation of the $FRET_{T\text{-}S}$ yield. Therefore, estimation of $R_{T\text{-}S}$ by precise measurement of ϕ_r^T and J considering $R_{S\text{-}S}$ is better to determine the real capability of the D as a good afterglow sensitizer. For a D with Φ_p = 0.01, ϕ_r^T becomes 1 if Φ_{ISC} is estimated to be 0.01. However, ϕ_r^T becomes 0.01 if Φ_{ISC} is estimated to be 1. The difference between these ϕ_r^T values causes a two-times difference of $R_{T\text{-}S}$ based on equation (5). However, the two-times difference of $R_{T\text{-}S}$ results in an approximately 10-times difference of $FRET_{T\text{-}S}$ when the volume is considered. Thus, accurate estimation of ϕ_r^T considering Φ_{ISC} is important to determine the real capability of proposed chemicals as triplet sensitizers. In addition, further analysis to distinguish the phosphorescence and TADF of a D is also necessary to consider real RT $FRET_{T\text{-}S}$, because separation of the two emission characteristics is possible by the temperature dependence of delayed emission.[93] The distinguishment of RTP and RT delayed fluorescence via two exciton and two excitation processes such as triplet-triplet annihilation process as a D could be done by checking excitation intensity dependence.[75] This analysis will also guide researchers to achieve more precise RT $FRET_{T\text{-}S}$.

This feature article focusing on FRET including logical discussion, as well as chemical examples from the viewpoint of the D, will be useful for not only guiding chemists to consider Ds for maximizing the capability of FRET involving triplet states, but it will also be useful for visualizing the current problems regarding the D for FRET involving triplet states. Although FRET involving triplet states contains a spin-flipping process, some aspects of the spin-flipping process are recently well understood from calculations.[94-97] Therefore, cooperative experimental and theoretical research considering the statistic correlation between the optically obtained results and calculational results is crucial to overcome the current limitations of FRET involving triplet states. Cooperative approaches could also be important for minimizing misunderstanding and leading to precise science. Hence, emerging future applications of FRET involving triplet excited

states in biology, as well as in optoelectronic devices via triplet harvesting, will be new avenues for research.

Conflicts of interest

There are no conflicts to declare.

Acknowledgments

This work was supported by Fusion Oriented REsearch for disruptive Science and Technology (FOREST) from the Japan Science and Technology Agency (JPMJFR201T) and JSPS KAKENHI (21H02011 and 21K18928).

Notes and references

1. C. W. Tang, S. A. VanSlyke and C. H. Chen, *J. Appl. Phys.*, 1989, **65**, 3610-3616.
2. J. Kido, M. Kimura and K. Nagai, *Science*, 1995, **267**, 1332-1334.
3. M. A. Baldo, M. E. Thompson and S. R. Forrest, *Nature*, 2000, **403**, 750-753.
4. H. Nakanotani, T. Higuchi, T. Furukawa, K. Masui, K. Morimoto, M. Numata, H. Tanaka, Y. Sagara, T. Yasuda and C. Adachi, *Nat. Commun.*, 2014, **5**, 4016.
5. S. Baluschev, T. Miteva, V. Yakutkin, G. Nelles, A. Yasuda and G. Wegner, *Phy. Rev. Lett.*, 2006, **97**, 143903.
6. D. N. Congreve, J. Lee, N. J. Thompson, E. Hontz, S. R. Yost, P. D. Reusswig, M. E. Bahlke, S. Reineke, T. Van Voorhis and M. A. Baldo, *Science*, 2013, **340**, 334-337.
7. D. E. J. G. J. Dolmans, D. Fukumura and R. K. Jain, *Nat. Rev. Cancer*, 2003, **3**, 380-387.
8. S. Hirata, K. Totani, T. Yamashita, C. Adachi and M. Vacha, *Nat. Mater.*, 2014, **13**, 938-946.
9. S. R. Adams, A. T. Harootunian, Y. J. Buechler, S. S. Taylor and R. Y. Tsien, *Nature*, 1991, **349**, 694-697.
10. M. Chalfie, Y. Tu, G. Euskirchen, W. W. Ward and D. C. Prasher, *Science*, 1994, **263**, 802-805.
11. A. Miyawaki, J. Llopis, R. Heim, J. M. McCaffery, J. A. Adams, M. Ikura and R. Y. Tsien, *Nature*, 1997, **388**, 882-887.
12. X. Y. Dai, M. Huo, X. Dong, Y. Y. Hu and Y. Liu, *Adv. Mater.*, 2022, **34**, e2203534.
13. H. Peng, G. Xie, Y. Cao, L. Zhang, X. Yan, X. Zhang, S. Miao, Y. Tao, H. Li, C. Zheng, W. Huang and R. Chen, *Sci. Adv.*, 2022, **8**, eabk2925.
14. N. J. Turro, *Modern Molecular Photochemistry*, University Science Books, Sausalito, CA, USA, 1991.
15. D. L. Dexter, *J. Chem. Phys.*, 1953, **21**, 836-850.
16. T. Förster, *Naturwissenschaften*, 1946, **33**, 166-175.
17. T. Förster, *Annalen der Physik*, 1948, **437**, 55-75.
18. T. Főrster, *Discussions of the Faraday Society*, 1959, **27**, 7-17.
19. B. Valeur, *Molecular Fluorescence: Principles and Applications*, Wiley-VCH Verlag GmbH, 2001.
20. B. W. van der Meer, *FRET – Förster Resonance Energy Transfer From Theory to Applications*, Wiley-VCH Verlag GmbH & Co. KGaA, 2014.
21. M. Irie, T. Fukaminato, T. Sasaki, N. Tamai and T. Kawai, *Nature*, 2002, **420**, 759-760.
22. E. Betzig, G. H. Patterson, R. Sougrat, O. W. Lindwasser, S. Olenych, J. S. Bonifacino, M. W. Davidson, J. Lippincott-Schwartz and H. F. Hess, *Science*, 2006, **313**, 1642-1645.
23. G. D. Scholes, *Annual Review of Physical Chemistry*, 2003, **54**, 57-87.
24. R. M. Clegg, in *Laboratory Techniques in Biochemistry and Molecular Biology*, Elsevier, 2009, **33**, 1-57.
25. J. R. Lakowicz, *Principles of fluorescence spectroscopy*, Springer, New York, 2006.
26. S. Hirata, *Adv. Opt. Mater.*, 2017, **5**. 1700116.
27. E. W. Schlag, S. Schneider and S. F. Fischer, *Annual Review of Physical Chemistry*, 1971, **22**, 465-526.
28. S. Hirata, *Appl. Phys. Rev.*, 2022, **9**. 011304.
29. S. K. Lower and M. A. El-Sayed, *Chem. Rev.*, 1966, **66**, 199-241.
30. S. Hirata, *J. Phys. Chem. Lett.*, 2018, **9**, 4251-4259.
31. P. N. Lai, C. H. Brysacz, M. K. Alam, N. A. Ayoub, T. G. Gray, J. M. Bao and T. S. Teets, *J. Am. Chem. Soc.*, 2018, **140**, 10198-10207.
32. I. Bhattacharjee and S. Hirata, *Adv. Mater.*, 2020, **32**, 2001348.
33. S. Hirata, K. Totani, J. Zhang, T. Yamashita, H. Kaji, S. R. Marder, T. Watanabe and C. Adachi, *Adv. Funct. Mater.*, 2013, **23**, 3386-3397.
34. S. Hirata, H. Hara and I. Bhattacharjee, *J. Phys. Chem. C*, 2020, **124**, 25121-25132.
35. L. Stryer, *Annual Review of Biochemistry*, 1978, **47**, 819-846.
36. E. A. Jares-Erijman and T. M. Jovin, *Nat. Biotech.*, 2003, **21**, 1387-1395.
37. T. Fukaminato, T. Sasaki, T. Kawai, N. Tamai and M. Irie, *J. Am. Chem. Soc.*, 2004, **126**, 14843-14849.
38. D. B. Clapp, *J. Am. Chem. Soc.*, 1939, **61**, 523-524.
39. V. B. Nazarov, V. I. Gerko and M. V. Alfimov, *Russ. Chem. Bull.*, 1996, **45**, 969-970.
40. V. L. Ermolaev and E. V. Sveshnikova, *Dokl. Akad. Nauk SSSR*, 1963, **149**, 1295.
41. R. G. Bennett, R. P. Schwenker and R. E. Kellogg, *J. Chem. Phys.*, 1964, **41**, 3040-3041.
42. R. E. Kellogg, *J. Chem. Phys.*, 1967, **47**, 3403-3406.
43. I. Isenberg, R. B. Leslie, S. L. Baird, R. Rosenbluth and R. Bersohn, *Proc. Natl. Acad. Sci.*, 1964, **52**, 379-387.
44. Y. Kubota, Y. Fujisaki and M. Miura, *B. Chem. Soc. Jpn.*, 1969, **42**, 853-853.
45. J. E. Wampler and J. E. Churchich, *Biochem. Biophys. Res. Commun.*, 1968, **32**, 629-634.
46. W. C. Galley and L. Stryer, *Biochemistry*, 1969, **8**, 1831-1838.
47. J. L. Risler, *Biochemistry*, 1971, **10**, 2664-2669.
48. T. A. Cha, A. H. Maki and J. C. Lagarias, *Biochemistry*, 1983, **22**, 2846-2851.
49. J. G. Weers and A. H. Maki, *Biochemistry*, 1986, **25**, 2897-2904.
50. G. B. Strambini, P. Cioni and P. F. Cook, *Biochemistry*, 1996, **35**, 8392-8400.
51. N. S. Allen, J. F. McKellar and D. Wilson, *J. Photochemi.*, 1977, **7**, 405-409.
52. P. Xue, P. Wang, P. Chen, B. Yao, P. Gong, J. Sun, Z. Zhang and R. Lu, *Chem. Sci.*, 2017, **8**, 6060-6065.
53. C. J. Chen, Z. G. Chi, K. C. Chong, A. S. Batsanov, Z. Yang, Z. Mao, Z. Y. Yang and B. Liu, *Nat. Mater.*, 2021, **20**, 175-180.
54. H.-T. Feng, J. Zeng, P.-A. Yin, X.-D. Wang, Q. Peng, Z. Zhao, J. W. Y. Lam and B. Z. Tang, *Nat. Commun.*, 2020, **11**, 2617.
55. Z. Wu, J. C. Roldao, F. Rauch, A. Friedrich, M. Ferger, F. Würthner, J. Gierschner and T. B. Marder, *Angew. Chem. Int. Edit.*, 2022, **61**, e202200599.
56. A. Cheng, Y. Jiang, H. Su, B. Zhang, J. Jiang, T. Wang, Y. Luo and G. Zhang, *Angew. Chem. Int. Edit.*, 2022, **61**, e202206366.
57. E. H. White and D. F. Roswell, *J. Am. Chem. Soc.*, 1967, **89**, 3944-3945.

58. D. R. Roberts and E. H. White, *J. Am. Chem. Soc.*, 1970, **92**, 4861-4867.
59. N. J. Turro, P. Lechtken, G. Schuster, J. Orell, H. C. Steinmetzer and W. Adam, *J. Am. Chem. Soc.*, 1974, **96**, 1627-1629.
60. M. A. Baldo, D. F. O'Brien, Y. You, A. Shoustikov, S. Sibley, M. E. Thompson and S. R. Forrest, *Nature*, 1998, **395**, 151-154.
61. M. A. Baldo, S. Lamansky, P. E. Burrows, M. E. Thompson and S. R. Forrest, *Appl. Phys. Lett.*, 1999, **75**, 4-6.
62. C. Adachi, M. A. Baldo, M. E. Thompson and S. R. Forrest. *J. Appl. Phys*., 2001, **90**, 5048-5051.
63. D. Chaudhuri, E. Sigmund, A. Meyer, L. Rock, P. Klemm, S. Lautenschlager, A. Schmid, S. R. Yost, T. Van Voorhis, S. Bange, S. Hoger and J. M. Lupton, *Angew. Chem. Int. Ed.*, 2013, **52**, 13449-13452.
64. H. Uoyama, K. Goushi, K. Shizu, H. Nomura and C. Adachi, *Nature*, 2012, **492**, 234.
65. Y. Liu, C. Li, Z. Ren, S. Yan and M. R. Bryce, *Nat. Rev. Mater.*, 2018, **3**, 18020.
66. A. R. Horrocks and F. Wilkinson, *Proceedings of the Royal Society of London. Series A, Mathematical and Physical Sciences*, 1968, **306**, 257-273.
67. D. Volyniuk, V. Cherpak, P. Stakhira, B. Minaev, G. Baryshnikov, M. Chapran, A. Tomkeviciene, J. Keruckas and J. V. Grazulevicius, *J. Phys. Chem. C*, 2013, **117**, 22538-22544.
68. K. Mori, T. P. M. Goumans, E. van Lenthe and F. Wang, *Phys. Chem. Chem. Phys.*, 2014, **16**, 14523-14530.
69. Y. Katsurada, S. Hirata, K. Totani, T. Watanabe and M. Vacha, *Adv. Opt. Mater.*, 2015, **3**, 1726-1737.
70. K. Fukasawa, Y. Sugawara, R. Tsuru, T. Yamashita and S. Hirata, *J. Phys. Chem. Lett.*, 2022, **13**, 7788-7796.
71. K. Ligi, E. Enkvist and A. Uri, *J. Phys. Chem. B*, 2016, **120**, 4945-4954.
72. A. Kirch, M. Gmelch and S. Reineke, *J. Phys. Chem. Lett.*, 2019, **10**, 310-315.
73. S. Kuila and S. J. George, *Angew. Chem. Int. Ed.*, 2020, **59**, 9393-9397.
74. S. Hirata and M. Vacha, *Adv. Opt. Mater.*, 2017, **5**, 1600996.
75. S. Kuno, H. Akeno, H. Ohtani and H. Yuasa, *Phys. Chem. Chem. Phys.*, 2015, **17**, 15989-15995.
76. B. Sk, R. Tsuru, K. Hayashi and S. Hirata, *Adv. Funct. Mater.*, 2023, **33**, 2211604.
77. K. Hayashi, K. Fukasawa, T. Yamashita and S. Hirata, *Chem. Mater.*, 2022, **34**, 1627-1637.
78. M. A. El-Sayed, *J. Chem. Phys.*, 1963, **38**, 2834-2838.
79. C.-Y. Chan, M. Tanaka, Y.-T. Lee, Y.-W. Wong, H. Nakanotani, T. Hatakeyama and C. Adachi, *Nat. Photonics*, 2021, **15**, 203-207.
80. L.-S. Cui, A. J. Gillett, S.-F. Zhang, H. Ye, Y. Liu, X.-K. Chen, Z.-S. Lin, E. W. Evans, W. K. Myers, T. K. Ronson, H. Nakanotani, S. Reineke, J.-L. Bredas, C. Adachi and R. H. Friend, *Nat. Photonics*, 2020, **14**, 636-642.
81. T. Higuchi, H. Nakanotani and C. Adachi, *Adv. Mater.*, 2015, **27**, 2019-2023.
82. A. Shahalizad, A. Malinge, L. Hu, G. Laflamme, L. Haeberlé, D. M. Myers, J. Mao, W. G. Skene and S. Kéna-Cohen, *Adv. Funct. Mater.*, 2020, **31**. 2007119.
83. M. Sun, J. Meng, W. Bao, M. Liu, X. Li, Z. Wang, Z. Ma, X. Wang and Z. Tian, *Chemphyschem*, 2022, DOI: 10.1002/cphc.202200716, e202200716.
84. A. S. Mathew, C. A. DeRosa, J. N. Demas and C. L. Fraser, *Anal. Methods*, 2016, **8**, 3109-3114.
85. H. Ohkita, W. Sakai, A. Tsuchida and M. Yamamoto, *Macromolecules*, 1997, **30**, 5376-5383.
86. R. Kabe and C. Adachi, *Nature*, 2017, **550**, 384-387.
87. F. Lin, H. Wang, Y. Cao, R. Yu, G. Liang, H. Huang, Y. Mu, Z. Yang and Z. Chi, *Adv. Mater.*, 2022, **34**, e2108333.
88. Y. Y. Hu, X. Y. Dai, X. Dong, M. Huo and Y. Liu, *Angew. Chem. Int. Ed.*, 2022, **61**, e202213097.
89. D. Wang, J. Gong, Y. Xiong, H. Wu, Z. Zhao, D. Wang and B. Z. Tang, *Adv. Funct. Mater.*, 2023, **33**. 2208895.
90. X. Zhang, M. Zeng, Y. Zhang, C. Zhang, Z. Gao, F. He, X. Xue, H. Li, P. Li, G. Xie, H. Li, X. Zhang, N. Guo, H. Cheng, A. Luo, W. Zhao, Y. Zhang, Y. Tao, R. Chen and W. Huang, *Nat. Commun.*, 2023, **14**, 475.
91. D. Li, Y. Yang, J. Yang, M. Fang, B. Z. Tang and Z. Li, *Nat. Commun.*, 2022, **13**, 347.
92. Y. Zhao, L. Ma, Z. Huang, J. Zhang, I. Willner, X. Ma and H. Tian, *Adv. Opt. Mater.*, 2022, **10**. 2102701.
93. F. B. Dias, T. J. Penfold and A. P. Monkman, *Methods and Applications in Fluorescence*, 2017, **5**, 012001.
94. N. Aizawa, Y. Harabuchi, S. Maeda and Y.-J. Pu, *Nat. Commun.*, 2020, **11**, 3909.
95. N. Aizawa, Y.-J. Pu, Y. Harabuchi, A. Nihonyanagi, R. Ibuka, H. Inuzuka, B. Dhara, Y. Koyama, K.-i. Nakayama, S. Maeda, F. Araoka and D. Miyajima, *Nature*, 2022, **609**, 502-506.
96. S. Hirata and I. Bhattacharjee, *J. Phys. Chem. A*, 2021, **125**, 885-894.
97. I. Bhattacharjee, K. Hayashi and S. Hirata, *JACS Au*, 2021, **1**, 945-954.